



# Synaptic Release Potentiation at Aging Auditory Ribbon Synapses

Thibault Peineau<sup>1,2†</sup>, Séverin Belleudy<sup>1†</sup>, Susanna Pietropaolo<sup>3</sup>, Yohan Bouleau<sup>1,2</sup> and Didier Dulon<sup>1,2\*</sup>

<sup>1</sup>Neurophysiologie de la Synapse Auditive, INSERM UMRS 1120, Bordeaux Neurocampus, Université de Bordeaux, Bordeaux, France, <sup>2</sup>Institut de l'Audition, Centre Institut Pasteur/Inserm, Paris, France, <sup>3</sup>INCIA, UMR 5287, CNRS, University of Bordeaux, Bat B2, Pessac, France

Age-related hidden hearing loss is often described as a cochlear synaptopathy that results from a progressive degeneration of the inner hair cell (IHC) ribbon synapses. The functional changes occurring at these synapses during aging are not fully understood. Here, we characterized this aging process in IHCs of C57BL/6J mice, a strain which is known to carry a cadherin-23 mutation and experiences early hearing loss with age. These mice, while displaying a large increase in auditory brainstem thresholds due to 50% loss of IHC synaptic ribbons at middle age (postnatal day 365), paradoxically showed enhanced acoustic startle reflex suggesting a hyperacusis-like response. The auditory defect was associated with a large shrinkage of the IHCs' cell body and a drastic enlargement of their remaining presynaptic ribbons which were facing enlarged postsynaptic AMPAR clusters. Presynaptic Ca<sup>2+</sup> microdomains and the capacity of IHCs to sustain high rates of exocytosis were largely increased, while on the contrary the expression of the fast-repolarizing BK channels, known to negatively control transmitter release, was decreased. This age-related synaptic plasticity in IHCs suggested a functional potentiation of synaptic transmission at the surviving synapses, a process that could partially compensate the decrease in synapse number and underlie hyperacusis.

**Keywords:** auditory hair cells, synaptic ribbons, synaptopathy, hyperacusis, Ca<sup>2+</sup> channels, exocytosis

## OPEN ACCESS

### Edited by:

Francesco Panza,  
University of Bari Aldo Moro, Italy

### Reviewed by:

Qiaojie Xiong,  
Stony Brook University, United States

Jun Li,  
Baylor College of Medicine,  
United States

### \*Correspondence:

Didier Dulon  
didier.dulon@inserm.fr

<sup>†</sup>These authors have contributed equally to this work and share first authorship

**Received:** 10 August 2021

**Accepted:** 21 September 2021

**Published:** 18 October 2021

### Citation:

Peineau T, Belleudy S, Pietropaolo S, Bouleau Y and Dulon D (2021) Synaptic Release Potentiation at Aging Auditory Ribbon Synapses. *Front. Aging Neurosci.* 13:756449. doi: 10.3389/fnagi.2021.756449

## INTRODUCTION

Age-related hearing loss (ARHL or presbycusis) is the most prevalent form of sensory disability in human populations and adversely affects the quality of life of many elderly individuals. Simultaneously with ARHL, chronic tinnitus and hyperacusis often develop due to abnormal neural activity in the central auditory system whose origin may arise from cochlear pathologies (for review see Knipper et al., 2013). The development of ARHL has been generally considered to be associated with primary degeneration of cochlear hair cells, with secondary deafferentation associating degeneration of spiral ganglion neurons and ribbon synapses. However, recent studies have resulted in a paradigm shift in the understanding of the early cause of ARHL (Kujawa and Liberman, 2015, 2019). During aging, hearing thresholds in the elderly often remain normal but speech intelligibility becomes hampered, especially in noisy environment. This pathology in the elderly is referred as hidden hearing loss and has been proposed to be caused in mice by an early loss of ribbon synapses contacting the inner hair cells (IHCs), well before any major loss of hair cells and spiral ganglion neurons (Stamatakis et al., 2006). While glutamate excitotoxicity, resulting in nerve terminal swelling, has been proposed to play a role in the setting of noise-induced hearing

loss (Pujol and Puel, 1999; Hu et al., 2020), the molecular mechanisms underlying the degeneration of the cochlear ribbon synapses during aging remain to be elucidated. Oxidative damage due to an increase in ROS levels seems to play a crucial role in ARHL (Fu et al., 2018) but how the ribbon synapses are functionally affected remain unknown.

The C57BL/6J inbred strain of mice has been extensively used as model for ARHL (Johnson et al., 1997; Spongr et al., 1997; Hequembourg and Liberman, 2001; Bartolome et al., 2002; Henry, 2002). This mouse strain carries a cadherin-23 mutation (*Cdh23*<sup>753A</sup>, also known as *Ahl*), which affects inner ear structures, characterized by progressive degeneration of ribbon synapses and spiral ganglion neurons, and results in age-related hearing loss. *Ahl* is a recessive single nucleotide mutation at 753 (G=>A) on the *Cdh23* gene on mouse chromosome 10 (Noben-Trauth et al., 2003). *Cdh23* encodes cadherin 23, a protein necessary for inner ear development and maintenance of the sensory hair cell structures, in particular the tip and lateral links of the stereocilia at the hair bundle (Siemens et al., 2004; Sollner et al., 2004; Lagziel et al., 2005; Michel et al., 2005; Kazmierczak et al., 2007), but growing anatomical evidence also suggests that synaptic rearrangements on sensory hair cells also contribute to auditory functional decline in C57BL/6J mice (Stamataki et al., 2006; Jiang et al., 2015; Zachary and Fuchs, 2015; Jeng et al., 2021). Surprisingly, aging C57BL/6J mice, although showing cochlear ribbon synapse degeneration and hearing loss, display increased acoustic startle reflex amplitudes (Ison and Allen, 2003; Ouagazzal et al., 2006; Ison et al., 2007) and a time increase in recovery from ABR short-term adaptation (Walton et al., 1995). Whether this exaggerated startle reflex can be explained by functional changes of cochlear hair cell ribbon synapses remain to be explored. Our present study will show that aged C57BL/6J mice, while losing nearly up to 50% of their IHC ribbon synapses, have IHCs with reduced BK channel clusters, larger remaining presynaptic ribbons (with increased Ca<sup>2+</sup> microdomains and larger sustained exocytotic responses) facing postsynaptic afferent boutons with larger AMPAR clusters. All these features indicated that synaptic release potentiation occurs at auditory IHC ribbon synapses during aging. This age-related synaptic plasticity could be viewed as compensatory mechanisms of the decrease IHC synapse number and may explain the hyperacusis-like startle reflex observed in aged C57BL/6J mice.

## RESULTS

### Increased ABR Thresholds and Hyperacusis-Like Effect on ASR

As previously described (Zheng et al., 1999; Zhou et al., 2006), CBA/J mice, used here as a reference, showed no sign of rapid degradation of their hearing function with aging, as attested by constant click ABR thresholds near 15 dB SPL up to 1 year

**Abbreviations:** ABR, Auditory brainstem responses; AHRL, Age-related hearing loss; ASR, Acoustic startle reflex; AZ, active zone; dB(SPL), decibel Sound Pressure Level; DPOAE, Distorsion product otoacoustic emission; IHC, Inner Hair Cell; OHC, Outer Hair Cell; ROS, reactive oxygen species; RRP, readily releasable pool; SRP, secondarily releasable pool.

of age (**Figure 1A**). On the contrary, C57BL/6J mice, carrying the *Cdh23*<sup>753A</sup> mutation, displayed an early progressive increase in ABR thresholds with aging (**Figure 1A**). Hearing thresholds started to increase significantly at postnatal day P180 to reach a mean 50 dB increase at P365 (click ABR thresholds above 65 dB SPL) as compared to young mature P30 mice. Distortion product otoacoustic emissions (DPOAEs) in P365 C57BL/6J mice were still present but significantly reduced, indicating that the electromechanical activity of the outer hair cells (OHCs) was also affected (**Figure 1D**). However, counting hair cells on surface preparations of organs of Corti from these P365 mice, in the mid-cochlea region (8–16 kHz), indicated only a moderate loss of OHCs and IHCs (statistically not significant; **Figure 2E**), in good agreement with the study of Zachary and Fuchs (Zachary and Fuchs, 2015). This moderate loss of OHCs suggested that the profound hearing loss occurring at P365 in C57BL/6J mice arose from additional factors than a simple alteration of the cochlear amplifier. We then compared the amplitude on the ABR wave-I as a function of sound intensity in young and old mice. The wave-I is known to result from the synchronous activity of the auditory nerve fibers and can provide an objective measure of ribbon synapses loss when measured at high sound intensity above 70 dB SPL. In P365 old mice, ABR wave-I amplitudes were largely reduced as compared to young mature P30 mice, even at high sound intensity when IHCs are directly stimulated and bypass the amplification process of the OHCs (**Figure 1B**). The large decrease in wave-I amplitude indicated a decreased number of auditory nerve fibers activated by sound and/or a decrease in their firing rate or synchrony. The latencies of the ABR wave-I were also significantly increased suggesting again that the IHC ribbon synapses are affected (**Figure 1C**).

Surprisingly, at lower sound intensities tested (between 20 and 35 dB above background noise level), the strength of the acoustic startle reflex (ASR) was found larger in old P365 C57BL/6J mice as compared to young P60, indicating hyperacusis reactivity (**Figure 1E**). The origin of this acoustic hypereactivity at low sound intensities could arise from central neural reorganization (Willott, 1996) and be consecutive to functional defect of the IHC ribbon synapses in aging C57BL/6J mice that we are going to characterize in this study. At loud sound intensities, 45 dB above background noise, the amplitudes of the ASR responses were however diminished in old mice, likely reflecting the increase in ABR thresholds due to a drastic decrease in the number of ribbon synapses per IHCs.

### Drastic Loss of IHC Synaptic Ribbons With Aging

Confocal immunofluorescence imaging of the synaptic ribbons in IHCs from C57BL/6J mice, in the cochlear region encoding between 8 and 16 kHz, showed a progressive and large decrease in the number of synaptic ribbons with aging, from 16.3 ± 0.3 ribbons/IHC at P15 to 8.7 ± 0.5 ribbons/IHC at P365 (**Figures 2A–C**). This nearly 50% loss of synaptic ribbons in IHCs of C57BL/6J mice at P365 was in good agreement with previous studies (Zachary and Fuchs, 2015; Jeng et al., 2020). Counting the spiral ganglion neurons in the mid-frequency

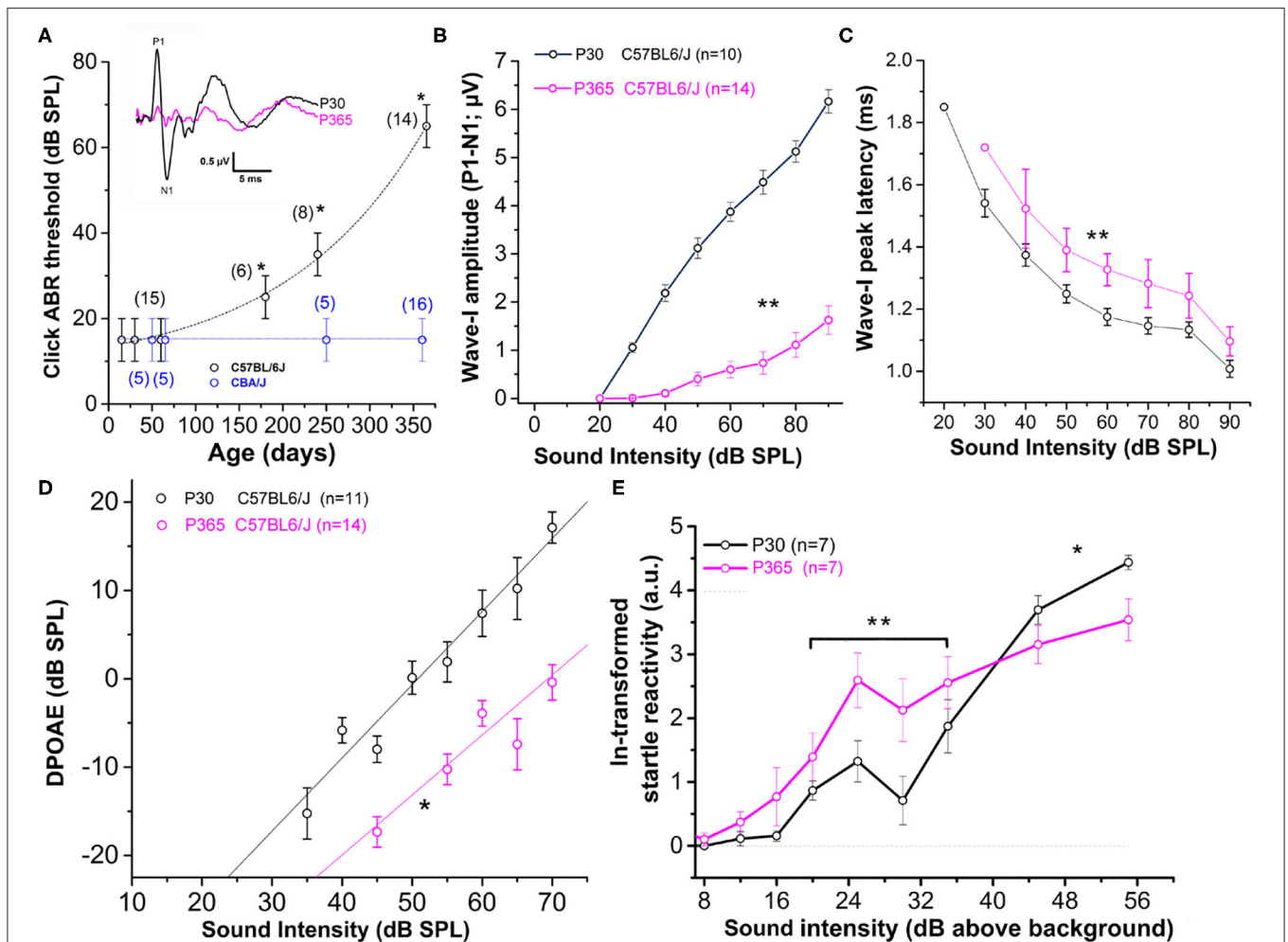


**FIGURE 1** | Sensorineural hearing loss with Aging in C57BL/6J mice. **(A)** Click-ABR thresholds as a function of age in CBA/J mice (blue;  $n = 5-16$ ) and C57BL/6J mice (black;  $n = 6-15$ ). For each strain, asterisks indicate significant difference with  $p < 0.05$  as compared to P30 mice (two-way ANOVA). Inset show comparative mean ABR waves at 70 dB SPL in P30 and P365 C57BL/6J mice. **(B)** Wave-I amplitude (P1-N1) as a function of sound intensity in young P30 (black) and old P365 (pink) C57BL/6J mice. Asterisks indicate significant difference with  $p < 0.05$  (two-way ANOVA;  $p = 0.001$ ). **(C)** Latency to reach peak amplitude of wave-I as a function of sound intensity. Significantly different with  $p = 0.003$  between 80 and 50 dB SPL (two-way ANOVA;  $n$  is indicated in graph **B**). **(D)** Distortion products otoacoustic emissions (DPOAEs;  $2f_1-f_2$  with  $f_1 = 12.73$  kHz and  $f_2 = 15.26$  kHz) as a function of sound intensity in young P30 (black) and old P365 (pink) C57BL/6J mice. Asterisk indicated significant difference with  $p < 0.05$  (two-way ANOVA,  $p = 0.01$ ). **(E)** Startle reactivity to acoustic stimulation. The intensity of startle reaction (in mV) was ln-transformed and obtained through two conditions of white-noise bursts of 20 and 40 ms. Note that below 35 dB above background the startle reaction is increased at P360 whereas at 45 and 55 dB above background the startle reaction is decreased compared to P30 mice. Asterisks indicated significant difference with  $p < 0.05$  (two-way ANOVA,  $p = 0.007$  between 20 and 35 dB and  $p = 0.005$  between 45 and 55 dB).

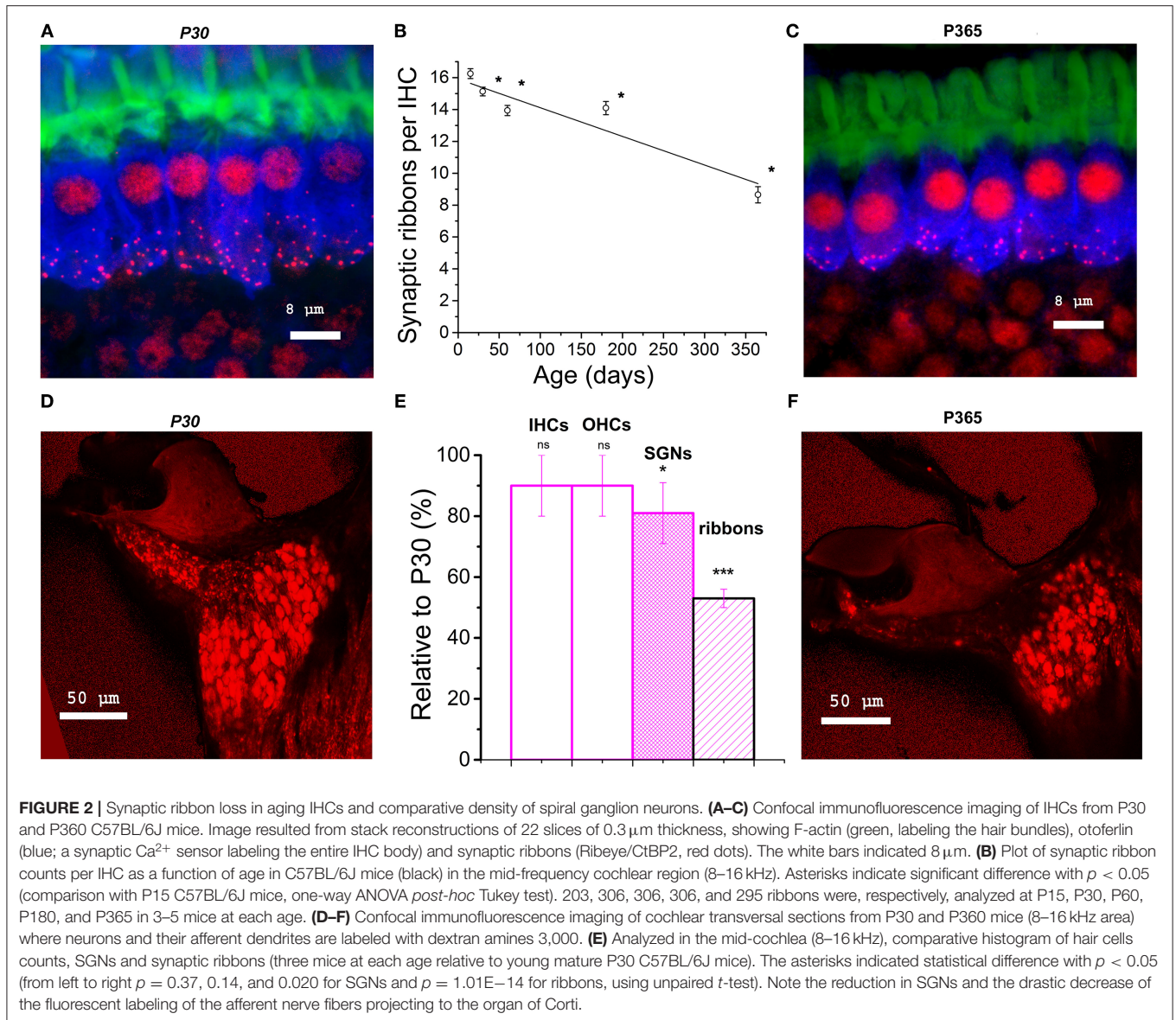
region of the cochlea (8–16 kHz) showed a mean 20% loss of neurons in P365 mice as compared to P30 mice (**Figures 2D–F**). Remarkably, the age-related loss of neurons, averaging 20%, was much less pronounced than the loss of IHC synaptic ribbons (50%), suggesting that there was a large number of neurons surviving without dendritic/synaptic projection toward the organ of Corti as previously shown by Stamatakis et al. (2006).

### Enlarged Presynaptic Ribbons Associated With Larger Postsynaptic AMPAR Clusters

When analyzing the 3-D imaging reconstruction of the IHC synaptic ribbons from P365 C57BL/6J IHCs from high resolution

confocal STED immunofluorescent sections, we found that these structures displayed a progressive increase in their mean size (volume) as compared to young P15 mice (**Figure 3A**). The mean volume of the synaptic ribbons increased nearly three-fold between P15 and P365 (**Figure 3B**). Interestingly, the increase in size of the ribbons started very early after P30, an age at which their number also started to decrease (**Figure 2B**) while hearing thresholds were still normal (**Figure 1A**).

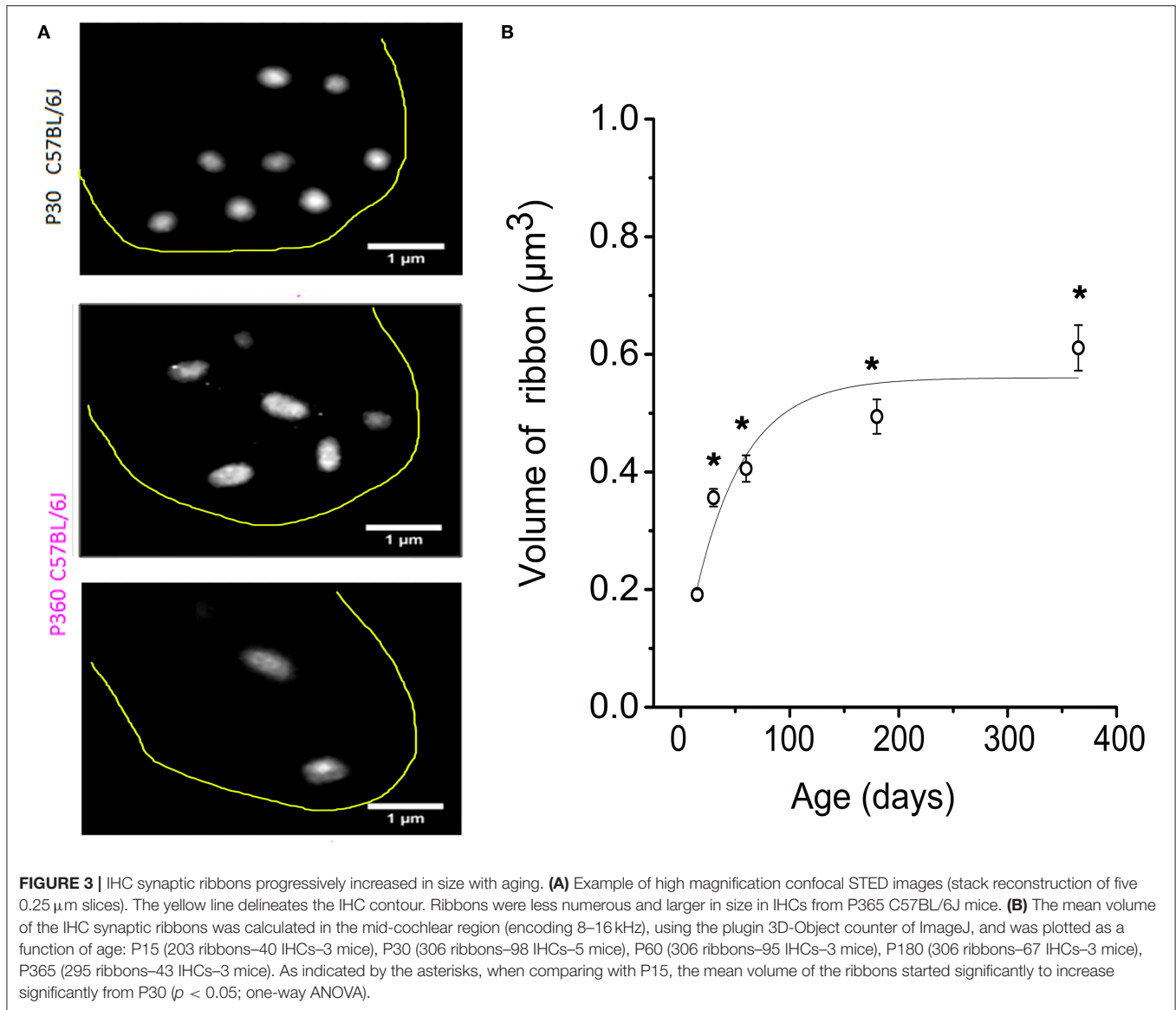
We next investigated the changes occurring with aging in the spatial distribution of the synaptic ribbons at the basolateral membrane of the IHCs. It is worth recalling that larger presynaptic ribbons associated to low-spontaneous-rate afferent



fibers are usually found at the modiolar side of the IHCs (i.e., the baso-lateral curved side of the IHCs directed toward the spiral ganglion neurons) while smaller ribbons associated with high-spontaneous-rate afferent fibers predominates at the pillar side (Liberman, 1982; Liberman et al., 2011). We found that, while a larger proportion of synaptic ribbons distributed at the modiolar side in young P30 IHCs ( $\sim 60\%$ ), the surviving ribbons in old P365 IHCs were evenly distributed at the pillar and modiolar side (**Figures 4A,B**). The loss of synaptic ribbons with aging was more pronounced at the modiolar side, i.e., at the side where most of the low-spontaneous (high threshold) fibers make contact to IHCs (**Figure 4C**). An increase in volume was noted both in pillar and modiolar ribbons (**Figure 4D**). Unlike young P30 IHCs, old P365 IHCs had modiolar and pillar ribbons with similar volume ( $0.7 \pm 0.1 \mu\text{m}^3$  and  $0.57 \pm 0.07 \mu\text{m}^3$ , respectively; not significantly different, unpaired *t*-test  $p = 0.28$ , **Figure 4D**).

Similar preferential loss of synaptic modiolar ribbons associated with an increase in ribbon volume was also reported after noise-induced hearing loss (Liberman and Kujawa, 2017; Hickman et al., 2020).

Postsynaptic afferent endings to ribbon IHCs express AMPA-type ionotropic glutamate [glutamate receptor A2 (GluA2)]-containing AMPA receptors (Matsubara et al., 1996; Hu et al., 2020). To determine whether the organization of postsynaptic AMPARs facing the IHCs ribbon was modified in old P365 mice we performed GluA2 immunostaining and confocal fluorescence imaging (**Figure 5**). As compared to young ribbon synapses, old synapses had larger ribbons associated with larger AMPAR clusters, suggesting that the changes occurring with aging are both at the pre and postsynaptic side in good agreement with the EM morphological analysis of Stamatakis et al. (2006).

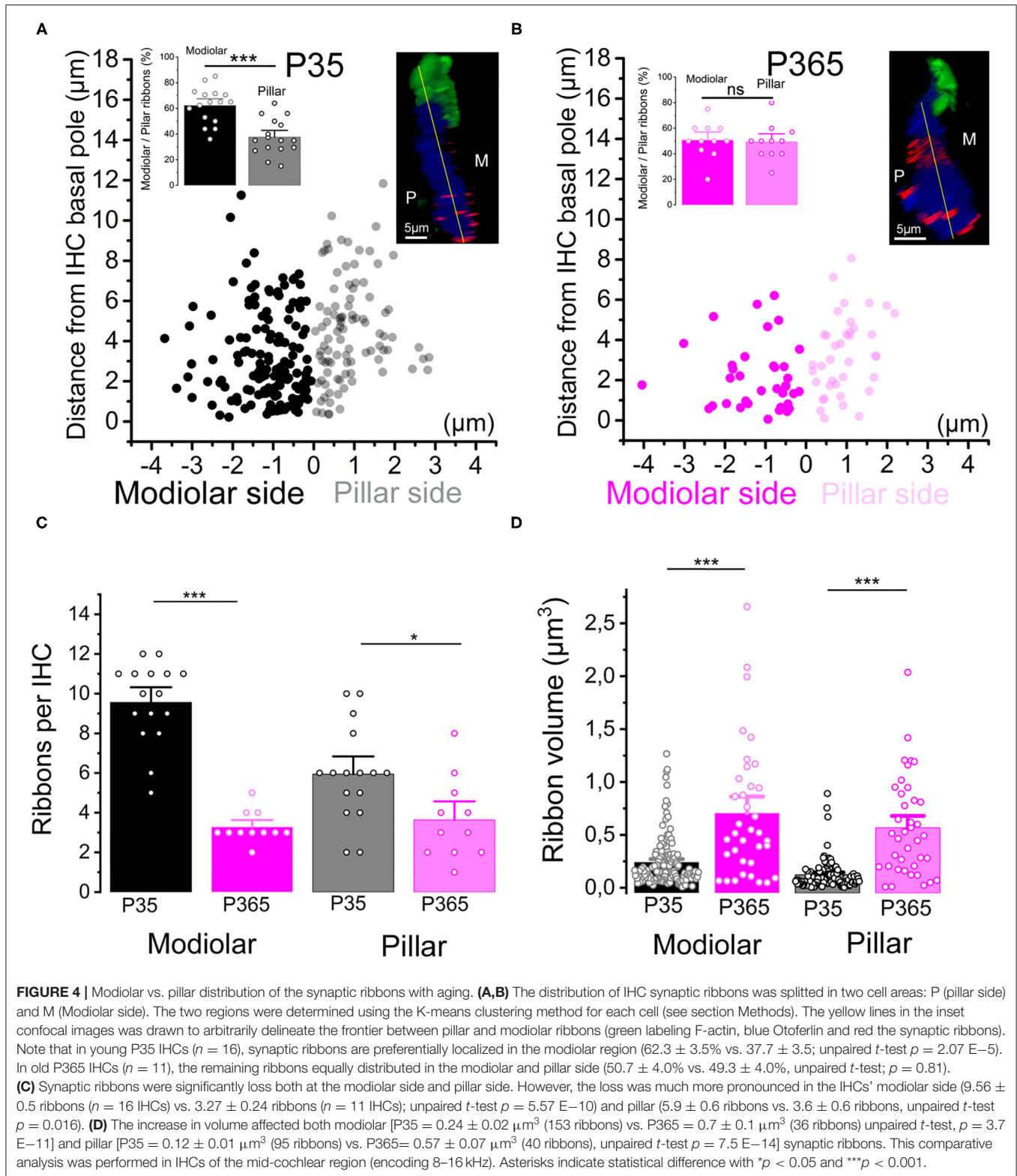


### Drastic IHC Cell Size Reduction With Aging

To determine whether the loss of synaptic ribbons was associated with a cell size reduction in old P365 IHCs, we labeled the cytosol of IHCs with an antibody against myo-7a, an unconventional myosin essential for the hair bundle functional integrity and found in the apical stereocilia as well as the cytoplasm of the hair cells (Hasson et al., 1995). We found a drastic reduction of the basal infra-nuclear synaptic zone of the IHCs from an average of  $15.7 \pm 0.1 \mu\text{m}$  ( $n = 34$ ) in P21 IHCs to  $12.4 \pm 0.3 \mu\text{m}$  ( $n = 50$ ) in old P365 IHCs (unpaired- $t$  test,  $p = 1.1 \text{E}-13$ , **Figures 6A–C**). The cell size reduction of old IHCs was confirmed by another method using whole-cell patch clamp measurement of the IHC resting membrane capacitance in organs of Corti preparation *ex-vivo* (**Figures 6D,E**). P365 IHCs displayed a significant smaller resting capacitance, measured at  $-70 \text{ mV}$ , of  $7.9 \pm 0.4 \text{ pF}$  ( $n = 22$ ) as compared to P21 IHCs ( $10.8 \pm 0.1 \text{ pF}$ ,  $n = 44$ , unpaired  $t$ -test,  $p = 3.7 \text{E}-10$ ).

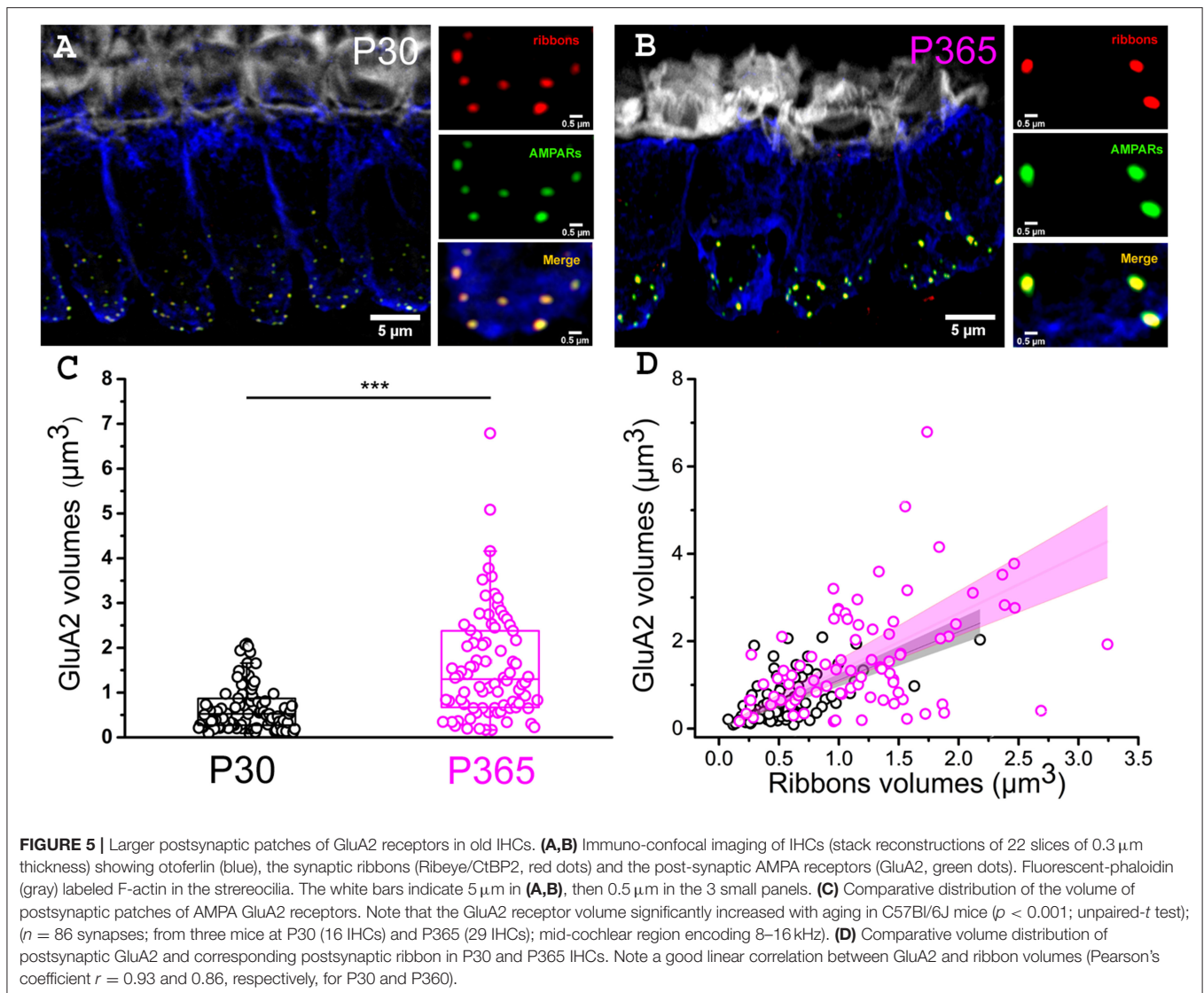
### Higher $\text{Ca}^{2+}$ Current Density and Exocytosis in Old IHCs

Although the loss of IHC ribbon synapses in C57BL/6J mice with aging is well-documented in the literature (Wan and Corfas, 2015), the functional changes of the remaining “old” IHC ribbon synapses has not yet been explored in detail at the cellular level. We investigated here the changes in the calcium-evoked exocytotic responses of aging IHCs from *ex-vivo* explants of the organ of Corti from aging C57BL/6J mice. We recall that  $\text{Ca}^{2+}$  is a key messenger for normal hearing since it tunes the transduction of the analogic sound signal into nerve impulses. This transduction occurs at the IHC synaptic active zone through the voltage-activation of  $\text{Ca}_v1.3 \text{ Ca}^{2+}$  channels (Brandt et al., 2003; Vincent et al., 2017) and the action of the  $\text{Ca}^{2+}$  sensor otoferlin (Roux et al., 2006; Beurg et al., 2010; Michalski et al., 2017). Increase in the density of L-type  $\text{Ca}^{2+}$  channels have long been recognized as a characteristic of aging central neurons



(Campbell et al., 1996; Thibault and Landfield, 1996) but possible altered function in  $\text{Ca}^{2+}$  signaling has not been investigated in aging IHCs.

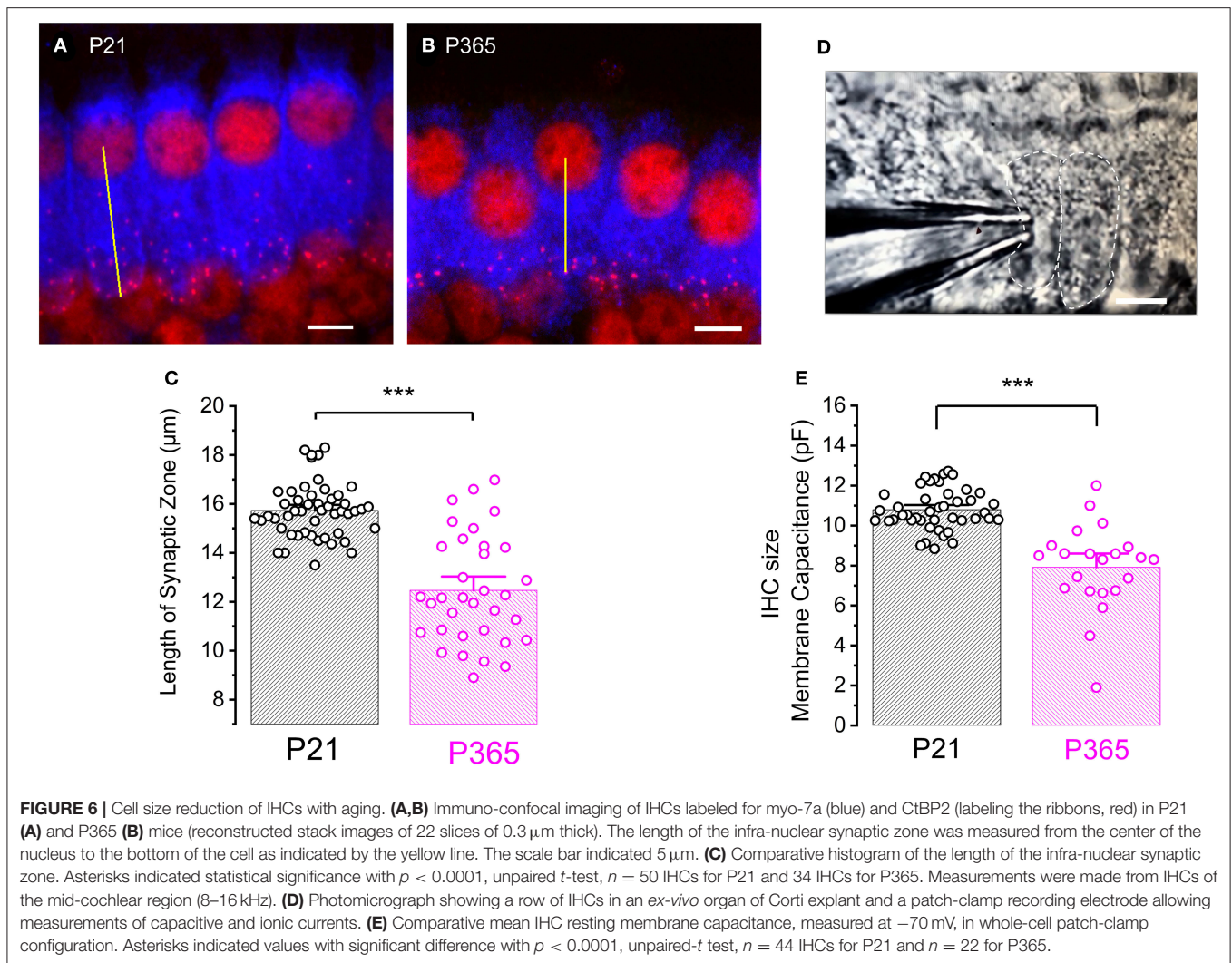
In the present study, whole cell patch-clamp recordings from old P365 IHCs showed a significantly increase in  $\text{Ca}^{2+}$  current density ( $\text{Ca}^{2+}$  current amplitude normalized to cell size) as



compared to young mature P30 IHCs, rising from a mean peak value of  $15.8 \pm 1.75$  pA/pF to  $20.1 \pm 1.9$  pA/pF at  $-10$  mV (**Figure 7A**; unpaired  $t$ -test,  $p < 0.05$ ). The voltage-activation curve of the  $\text{Ca}^{2+}$  currents in old P365 IHCs remained similar to the young mature P30 IHCs, with a mean half-voltage activation ( $V_{1/2}$ ) of  $-29.3 \pm 1.1$  and  $-26.7 \pm 2.8$  mV, respectively (unpaired  $t$ -test,  $p = 0.06$ ).

Patch-clamp measurement of membrane capacitance upon depolarizing voltage-steps from  $-80$  to  $-10$  mV with increasing time duration allowed to compare the kinetics of vesicle exocytosis in young and old IHCs. For brief stimulations below 25 ms, a time-frame addressing the release of the Readily Releasable Pool (RRP) of vesicles, the exocytosis response (normalized to cell size) was similar in P30 and P365 IHCs (**Figures 7B,C**). However, longer depolarization above 25 ms revealed a more sustained exocytotic response in old IHCs, suggesting the mobilization of a more efficient secondarily releasable pool (SRP), i.e., a more efficient vesicle recruitment in

these cells (**Figures 7B,D**). To investigate whether this increased SRP exocytosis was due to higher  $\text{Ca}^{2+}$  microdomains at the ribbon active zones, we used the high affinity  $\text{Ca}^{2+}$ -indicator Rhod-2 ( $K_d = 570$  nM) which is known to allow a good monitoring of low  $\text{Ca}^{2+}$  concentrations ranging from 20 nM to 20  $\mu\text{M}$  (Del Nido et al., 1998). We choose to use Rhod-2 rather than a low affinity  $\text{Ca}^{2+}$  dye such as OGB-5N with a  $K_d$  at 20  $\mu\text{M}$  (Vincent et al., 2014) because we wanted here to primarily probe the amplitude of the  $\text{Ca}^{2+}$  microdomains, where the changes in  $\text{Ca}^{2+}$  concentrations are due to  $\text{Ca}^{2+}$  diffusion and are lower than at the nanodomain range near the  $\text{Ca}^{2+}$  channels.  $\text{Ca}^{2+}$  microdomains allow vesicle replenishment, a process occurring at the  $\mu\text{m}$  scale away from the ribbon and their associated  $\text{Ca}^{2+}$  channels (Spassova et al., 2004; Johnson et al., 2005; Graydon et al., 2011). We found that, upon 5 consecutive long 100 ms voltage-step stimulations (from  $-80$  to  $-10$  mV), IHCs displayed brighter transient  $\text{Ca}^{2+}$  hot spots (measured in 1  $\mu\text{m}^2$  areas) at their basal synaptic area in P365 mice as



compared to young P30 IHCs (**Figures 8A,B**). This indicated the expression of synaptic  $\text{Ca}^{2+}$  microdomains with larger amplitude in old P365 IHCs, a response likely due to a larger  $\text{Ca}^{2+}$  channel density at their ribbon active zones (**Figure 7A**). Simultaneously, in the same cells, the application of the 5 consecutive 100 ms stimulations, generated a facilitated vesicular recruitment in old P365 IHCs (**Figure 8D**). Also, as a consequence of increased  $\text{Ca}^{2+}$  microdomains in old IHCs, the simultaneous recording of  $\text{Ca}^{2+}$  currents showed an enhanced time-inactivation, indicative of an increased  $\text{Ca}^{2+}$ -dependent inactivation due to higher intracellular  $\text{Ca}^{2+}$  concentration (**Figure 8C**).

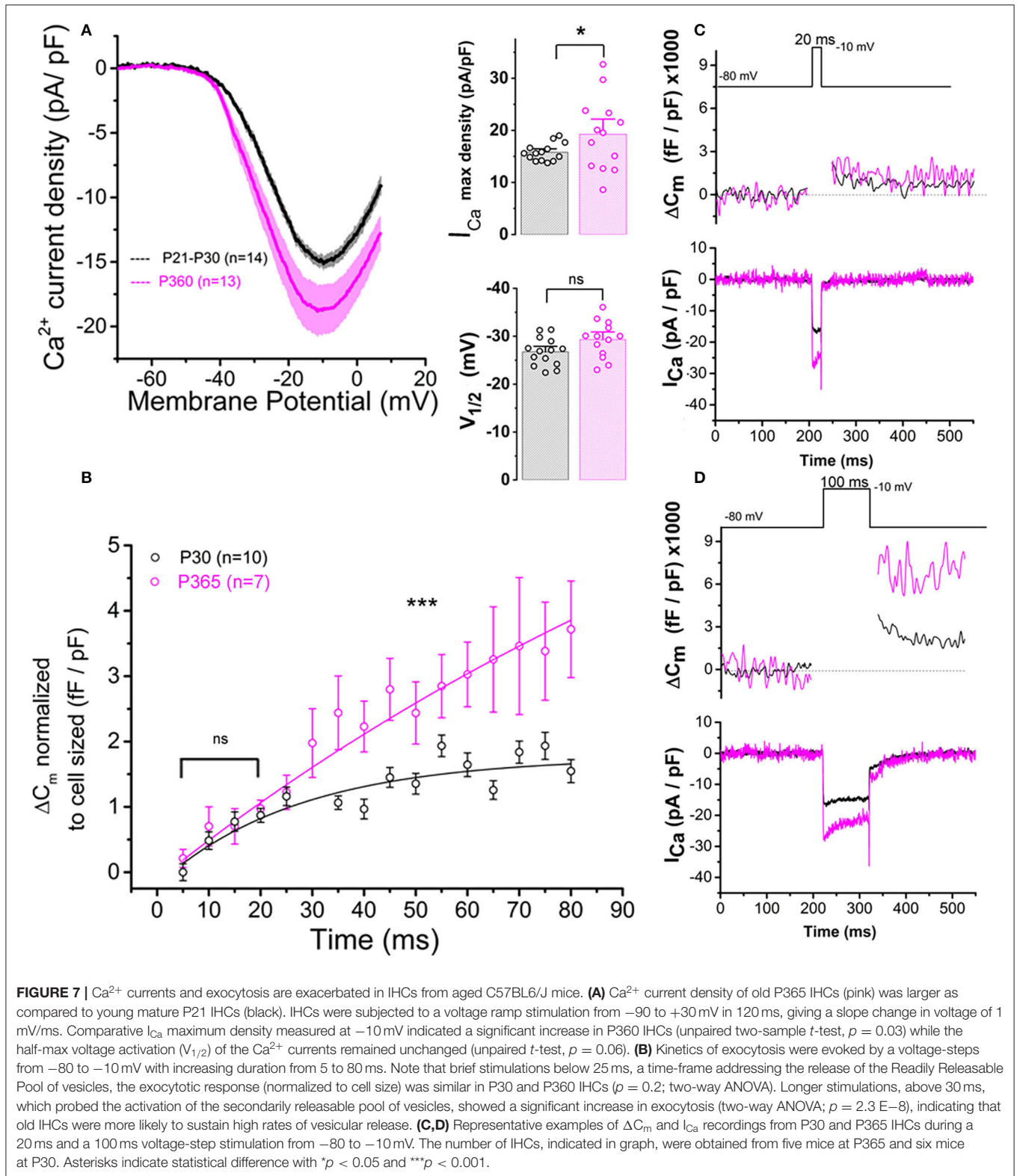
### Aging Promoted Autophagy in IHCs Through the Recruitment of LC3B

The size reduction of the old IHCs (**Figure 6**) suggested that the degenerative process of the ribbon synapses was associated with a concomitant reduction of the cell surface membrane of IHCs during aging, suggesting a largely augmented uptake of plasma membrane through endocytosis. Like other type of cells, such as neurons or retinal cells, auditory hair cells utilize autophagic pathways to maintain cell homeostasis during

excessive ROS production (Fu et al., 2018; Defourny et al., 2019). Autophagy is a degradation process where cytoplasmic and plasma membrane components are engulfed by vesicles called autophagosomes. To determine whether this process could explain the IHC size reduction with aging, we investigated the recruitment of LC3B, a structural protein of autophagosomal membranes. We assessed and compared the autophagosome numbers and surface area in young P30 and old P365 IHCs by quantifying LC3B puncta numbers/cell by using confocal immunofluorescence. We found that the number and overall surface area of LC3-positive structures in IHCs largely increased with aging (**Figure 9**), indicating an increased autophagosome formation. Similar investigations in P365 CBA/J mice, a strain which does not display early age-related hearing loss (**Figure 1**), showed a weak expression of LC3B in IHCs (**Figure 9**).

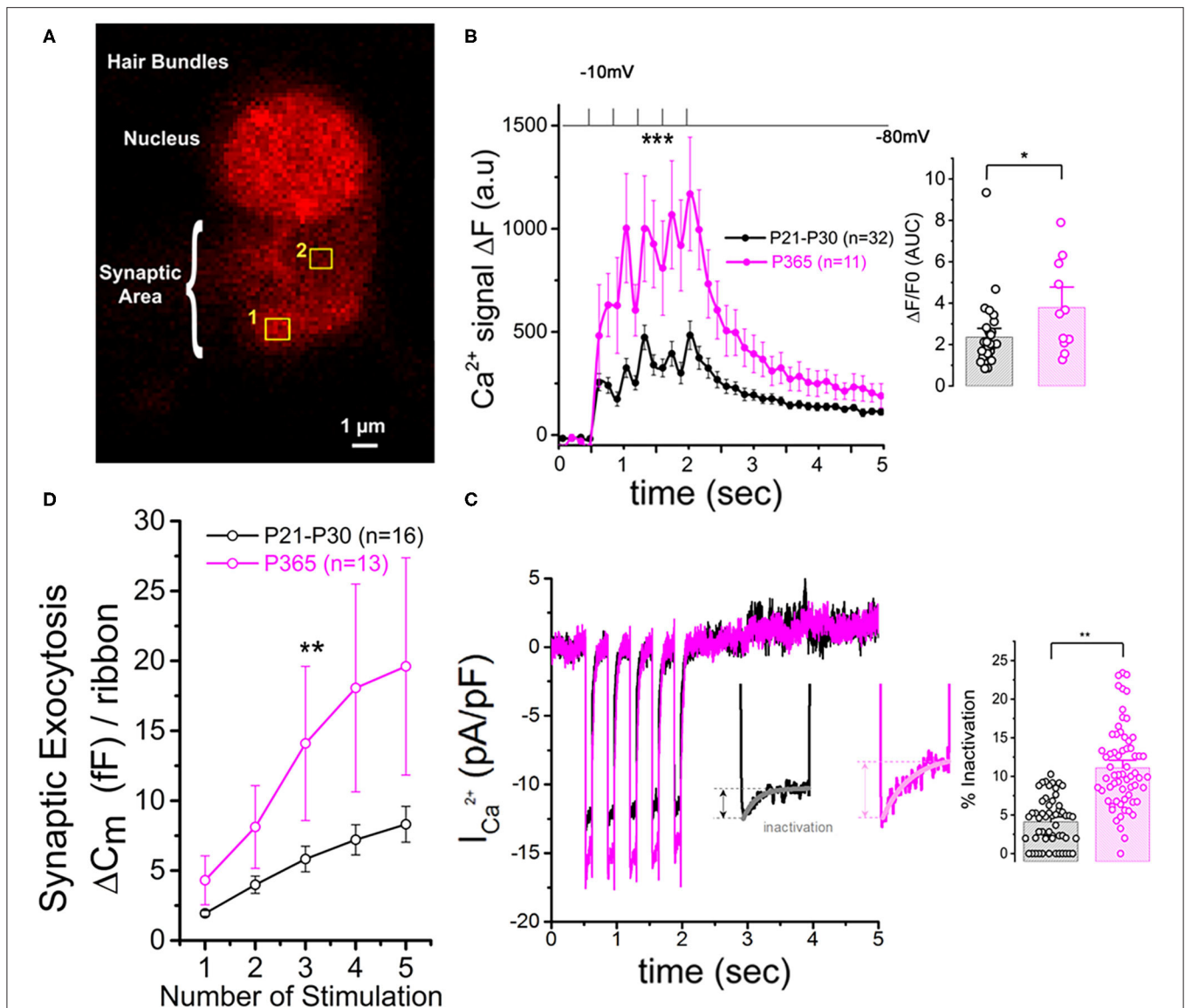
### Clustering and Voltage-Dependent Activation of BK Channels Are Affected in Aging IHCs

There is increasing evidence that oxidative damage due to an increase in ROS levels plays a crucial role in age-related



degeneration of the synaptic ribbon synapses (Fu et al., 2018; Rousset et al., 2020). BK ( $\text{K}_{\text{Ca}1.1}$ ) channels are known to be highly sensitive to oxidative stress and their activity is a good indicator

of intracellular ROS production (Sahoo et al., 2014; Hermann et al., 2015). Interestingly, a decrease in BK channel expression in IHCs has been associated to noise-related ROS and peroxysome



pathology (Delmagnani et al., 2015) but never yet described in IHCs during age-related hearing loss. It is worth recalling that BK channels allow fast repolarization of IHCs and are essential for phase-locking of the auditory afferent neurons (Kros et al., 1998; Skinner et al., 2003; Oliver et al., 2006; Kurt et al., 2012). We here investigated, using immunofluorescent confocal microscopy, the comparative level expression of BK channels in IHCs from young (P30) and old P365 C57BL/6J mice. In young mature IHCs, BK channels are known to be organized in a dozen of clusters at the neck of the IHCs below the cuticular plate (Pyott et al., 2004; Hafidi et al., 2005). We used 3-D reconstructions from stacks of confocal images of immunostained organs of Corti (mid-cochlear

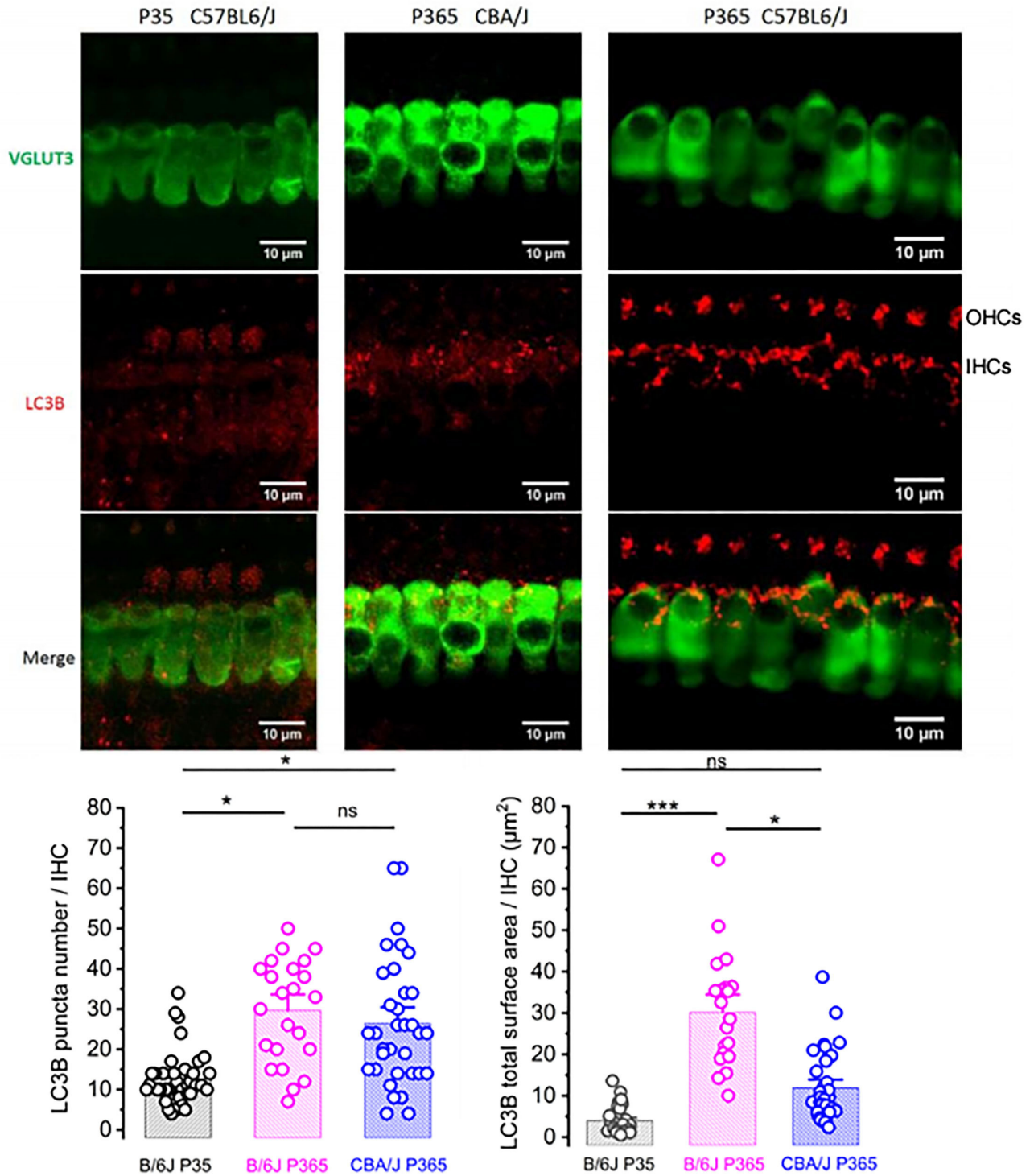
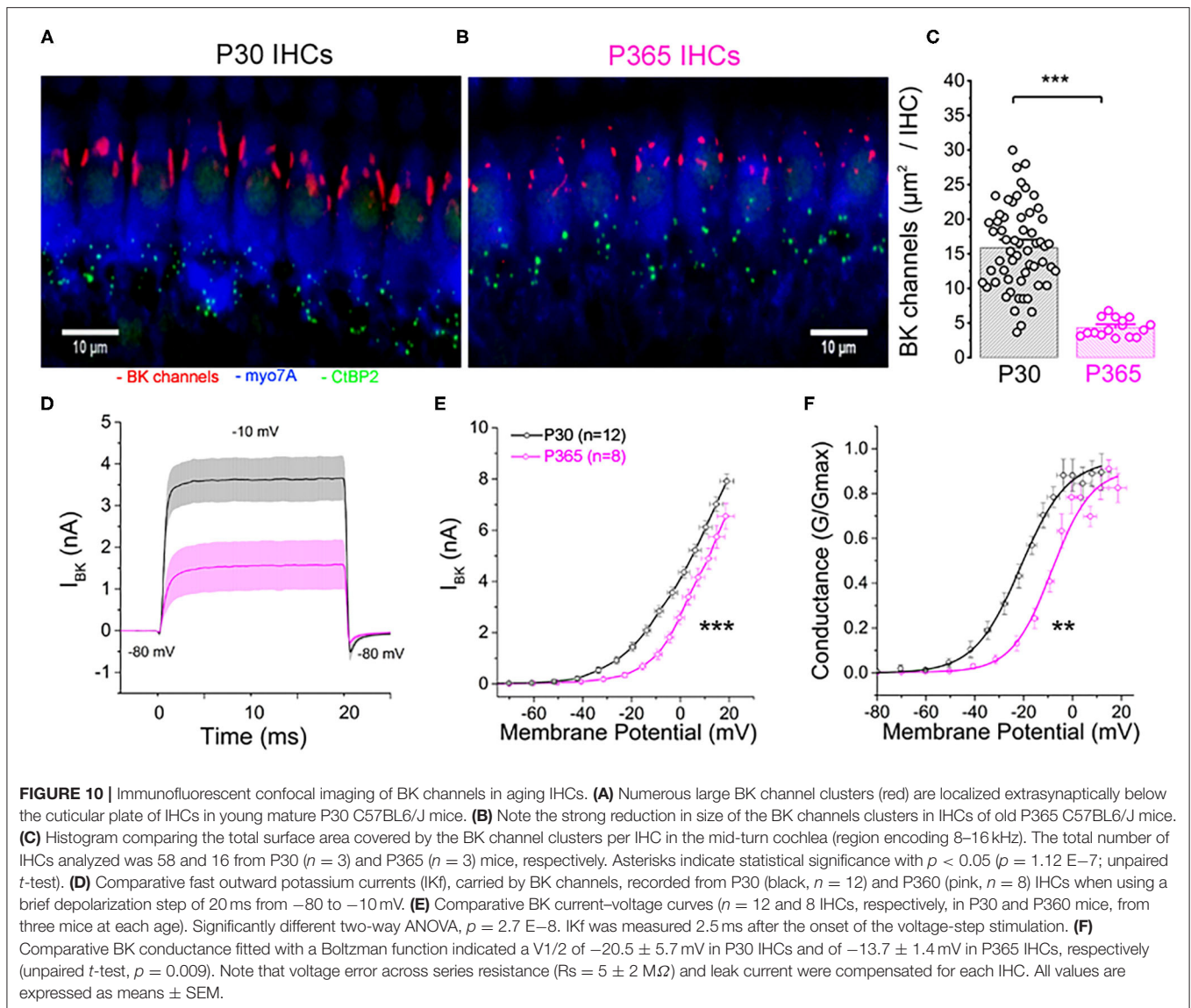


**FIGURE 9** | LC3B-positive structures are prominent in aging IHCs. Representative confocal immunofluorescence images showing LC3B staining in IHCs from young P30 C57BL/6J (left), old P365 CBA/J (middle), and old P365 C57BL/6J (right) mice. The histograms below show the quantification of the LC3B puncta average number and average mean surface area per IHC. Images were obtained from processing confocal stack images (22 of 0.3 µm thickness) using ImageJ quantification tool (3D-object counter). Quantification was performed from 23 to 38 IHCs for each condition in the mid-cochlea (encoding region 8–16 kHz; 3 mice). Asterisks indicate statistical significance  $p < 0.05$  (unpaired  $t$ -test).



frequency region 8–16 kHz) to determine the mean total surface area of the BK clusters per IHCs (**Figures 10A–C**). The results indicated that the membrane surface covered by BK channel clusters was reduced almost three-fold in P365 IHCs as compared to P30 IHCs.

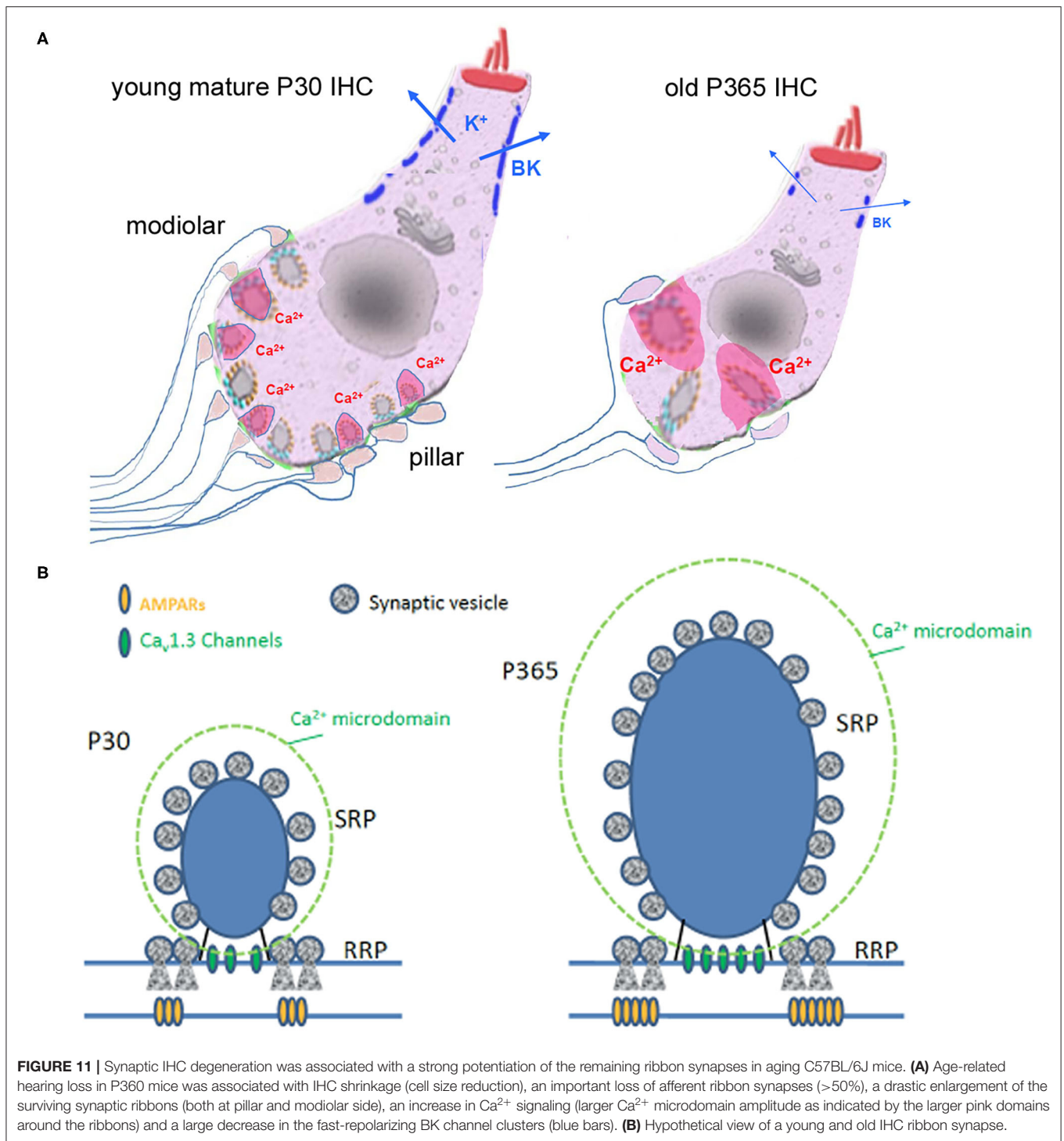
To further characterize the changes in BK channel function with aging, we performed whole cell patch-clamp recordings in IHCs from P30 and P365 mice. Since BK currents in IHCs have the peculiar property to be extremely fast activating currents (also termed  $I_{Kf}$ ; Kros et al., 1998), these currents were recorded during brief 20 ms depolarizing steps and measured 2.5 ms after their onset (**Figures 10D–F**). BK currents in IHCs from young mature have also the particularity to activate at extremely negative membrane potential (near  $-60$  mV) (Lingle et al., 2019). While the whole-cell conductance of BK channels from P365 IHCs was not significantly different from P30 IHCs ( $0.26 \pm 0.04$  nS and  $0.23 \pm 0.03$  nS, respectively), their voltage-dependant

activation showed a large positive shift of 7 mV (**Figure 10F**). Interestingly, the decrease in size of the BK patches and the positive voltage-activation shift in old IHCs somewhat resembled the phenotype observed in mice KO for LRRC52, a  $\gamma$  BK regulatory subunits (Lang et al., 2019; Lingle et al., 2019), suggesting that the BK complex formed with this  $\gamma$  subunit could be one the target of the degenerative oxydative process in aging C57BL56/J mice IHCs.

## DISCUSSION

### Larger Synaptic Ribbons Associated With Increased $\text{Ca}^{2+}$ Signals

Ribbons are presynaptic organelles tethering glutamate-filled vesicles at the hair cell active zone (AZ, **Figure 11**). These intracellular structures, composed of the protein RIBEYE, are



anchored by the scaffold protein bassoon to the AZ plasma membrane, adjacent to  $Ca^{2+}$   $Ca_v1.3$  channels (Brandt et al., 2003; Graydon et al., 2011; Jing et al., 2013; Vincent et al., 2017). Ribbons are essential for high rate of transmitter release and for high temporal precision of neuronal encoding of sound at the auditory afferent nerve fibers (Becker et al., 2018; Jean et al., 2018). Each auditory IHC have 10 to

20 synaptic ribbons depending of their cochlear frequency location (Meyer et al., 2009). Ribbons are heterogeneous in size and each ribbon makes a single synaptic contact with one afferent nerve fiber. Remarkably, fibers associated to large ribbons display low spontaneous rate and high-threshold have the tendency to be distributed at the modiolar side of IHCs (Liberman et al., 2011). Nerve fibers associated

with smaller ribbons display high spontaneous rate and low-threshold activation, are mainly located toward the pillar side of IHCs. Interestingly, we found here that old C57BL/6J IHCs preferentially loose modiolar ribbons (known to be associated with high threshold low spontaneous fibers), therefore mimicking what is happening during noise-induced hearing loss (Fernandez et al., 2015; Liberman and Kujawa, 2017; Hickman et al., 2020). Heterogeneity in the voltage-dependence of  $\text{Ca}^{2+}$  channels and release site coupling has been recently proposed to contribute to the firing fiber specificity, with modiolar ribbons being activated at more negative potentials (Ozçete and Moser, 2021). In our study, we did not find evidence for a voltage-shift in the voltage-dependence of  $\text{Ca}^{2+}$  channels with aging but we did observe an increase in the density of  $\text{Ca}^{2+}$  currents. The increase in  $\text{Ca}^{2+}$  entry was further confirmed by the stronger time-inactivation of the  $\text{Ca}^{2+}$  currents (Grant and Fuchs, 2008; Vincent et al., 2017).

One of the most striking observations was that the IHC synaptic ribbons underwent a nearly three-fold increase in size with aging, confirming a certain degree of plasticity of these synaptic structures. The enlargement of the presynaptic ribbons was in good agreement with a previous ultrastructural study in aging C57BL/6J mice by Stamatakis et al. (2006) and the recent study of Jeng et al. (2020). Interestingly, the size of the young mature IHC synaptic ribbons is known to correlate positively with the AZ  $\text{Ca}^{2+}$  microdomain amplitude, as well as the number and gating of the  $\text{Ca}_v1.3$   $\text{Ca}^{2+}$  channels (Frank et al., 2009; Neef et al., 2018). Also, hair cells of transgenic zebrafish with enlarged ribbons display larger ribbon-localized  $\text{Ca}^{2+}$  currents (Sheets et al., 2017). In agreement with these previous studies, we found here, in IHCs from aging C57BL/6J mice, that the remaining larger ribbons were associated with larger  $\text{Ca}^{2+}$  microdomain amplitude, and larger density of calcium currents, reinforcing the idea that  $\text{Ca}^{2+}$  ions regulate the size of the synaptic ribbons. In this context, it is worth recalling that mitochondrial- $\text{Ca}^{2+}$  uptake has been proposed to lower cellular  $\text{NAD}^+/\text{NADH}$  redox and regulates ribbon size, possibly by acting through the  $\text{NAD}^+$  binding site of the B domain of RIBEYE (Wong et al., 2019). *In vitro* work has shown that  $\text{NAD}^+$  and  $\text{NADH}$  can promote interactions between ribeye domains (Magupalli et al., 2008) and the size of the ribbons would be then sensitive to the subcellular synaptic  $\text{NAD}^+/\text{NADH}$  redox level (Wong et al., 2019), suggesting that the increase in size of the IHCs ribbons from aged C57BL/6J mice also results from  $\text{NAD}^+/\text{NADH}$  homeostasis disruption.

### Increased Capacity for Sustained IHC Synaptic Exocytosis: Implication for the Discharge Pattern of the Auditory Nerve Firing

As a consequence of larger  $\text{Ca}^{2+}$  microdomains, we found that IHCs from old C57BL/6J mice had larger and more sustained exocytotic responses. These larger release responses could also well be explained by a higher synaptic vesicle density at the active zone of the IHC ribbon synapses as suggested by the EM study

of Stamatakis et al. (2006). Surprisingly, the recent study of Jeng et al. (2020), which did not perform  $\text{Ca}^{2+}$  imaging, concluded that the size and kinetics of  $\text{Ca}^{2+}$ -dependent exocytosis in IHCs were unaffected in aging mice but this study did not normalize the IHC exocytotic responses to their cell size or to their ribbon synapse number, and therefore may have overlooked the differential phenotype.

What would be the consequences on the discharge pattern of the remaining afferent fibers of a more sustained release capacity in old ribbon synapses? Fast adaptation in the discharge rate of the afferent auditory nerve fibers is thought to be one of their essential property for emphasizing the timing information of sound stimuli. This adaptation takes the form of a fast increase in spike rate at stimulus onset that rapidly declines in a double exponential decay to a lower steady-state rate after a few tens of milliseconds (Taberner and Liberman, 2005). The origin of this fast adaptation has been proposed to arise first from  $\text{H}^+$  release block of  $\text{Ca}^{2+}$  channels and second to rapid depletion of synaptic vesicle release (Vincent et al., 2017). We predict that the increased capacity to sustain SRP exocytosis in old IHCs with larger ribbons would have the tendency to decrease the level of firing adaptation of the auditory fibers and therefore explain the altered recovery from short-term adaptation in old C57BL/6J mice (Walton et al., 1995).

Furthermore, we confirmed here the hyperacusis-like effect of the startle responses in old C57BL/6J mice (Ison et al., 2007). This increased response at low sound intensity could be explained by a release potentiation at the IHC ribbon synapses due to the presynaptic higher  $\text{Ca}^{2+}$  channel density associated with a larger ribbon coupled with a larger vesicular SRP, and increased expression of post-synaptic AMPARs. All these features would make the auditory ribbon synapses hypersensitive and underlie the hyperacusis-like reflex in old C57BL/6J mice.

### IHC Shrinkage and Disruption of BK Channel Clusters

Another novel observation of our study was the drastic reduction in cell size of IHCs from aging C57BL/6J mice. Interestingly, tuberous sclerosis rapamycin-sensitive complex 1 (mTORC1) has been shown to be overactivated and promote oxidative damages to synapse ribbon loss in aging C57BL/6 mice (Fu et al., 2018). We found that aged P365 IHCs had an increase expression of the autophagy marker LC3B. The activation of the mTOR pathway with aging could therefore trigger the cell size reduction of IHCs, by activating the autophagy pathway, as proposed in many other cell types (Fingar et al., 2002; Fumarola et al., 2005). In addition, our study described another novel remarkable feature of aging IHCs, a drastic disruption of the BK channel clusters, suggesting that these potassium channels are also a good indicator of the redox state and autophagy in IHCs. The expression and distribution of BK channels could be regulated through the rapamycin insensitive mTOR complex 2 (mTORC2) as shown in the kidney glomerulus podocytes (Wang et al., 2019). Interestingly, the disruption of the BK channel clusters in aging IHCs was associated with a large positive

shift in their voltage-activation curve, suggesting that the fast-repolarizing property mediated by BK channels which likely contributes to decrease transmitter release (Skinner et al., 2003), would be largely hampered during sound stimuli in aging mice, an additional factor that may also contribute to hyperacusis.

## A Role of Cadherin-23 in Ribbon Synapse Maintenance and Function?

In the CNS, cadherins are considered as essential  $\text{Ca}^{2+}$ -binding transmembrane cell adhesion molecules that regulate synapse formation and function (Bamji, 2005). In the murine retina, cadherin-23 is highly abundant at the ribbon synapse of rod photoreceptor cells (Bolz et al., 2002). The presence of cadherin-23 at IHC ribbon synapses remain unknown. The results observed by our study and others in C57BL/6J mice suggest that this molecule plays a crucial role in hair cell ribbon synapse maintenance and function. It is possible that the *Cdh23*<sup>753A</sup> mutation weakens the mechanical organization of the hair cell synaptic contacts leading with aging to their progressive disorganization. The exacerbated release of glutamate in aging ribbon synapses could then lead to excitotoxicity and progressive synapse degeneration.

## CONCLUSIONS

In conclusion, our study unraveled several novel functional and structural features of aging in IHC ribbon synapses from C57BL/6J mice (Figure 11): (1) a large reduction in IHC cell size, (2) a drastic enlargement of the presynaptic ribbons and postsynaptic AMPAR clusters, (3) an increased presynaptic  $\text{Ca}^{2+}$  signaling associated with a stronger sustained exocytotic response, and (4) a disruption of BK channel clusters and a drastic shift in their voltage-dependence decreasing their potential negative feedback on neurotransmission. Overall, these results suggested that aging IHCs ribbon synapses can undergo important structural and functional plasticity that led to synaptic potentiation that could explain the paradoxical hyperacusis-like exaggeration of the acoustic startle reflex observed in C57BL/6J mice.

## MATERIALS AND METHODS

### Mice

Inbred C57BL/6J mice of either sex (Souris JAX<sup>TM</sup> C57BL/6J, Jackson Laboratory) which are homozygous for the recessive cadherin-23 mutation *Cdh23*<sup>753A</sup> (also known as Ah1) were used in the present study. Hearing thresholds and IHC ribbon counts in mice of either sex were performed at postnatal ages: P15, P30, P60, P180, and P365. CBA/J mice of either sex (from Charles River) were also tested as controls at P50, P250, and P365. Animal care and all procedures were approved by the institutional care and use committee of the University of Bordeaux and the French Ministry of Agriculture (agreement C33-063-075).

### Assessment of Hearing Thresholds (ABRs)

To record ABRs (Auditory Brainstem Responses, which represent the sound-evoked synchronous firing of the auditory

cochlear nerve fibers and the activation of the subsequent central auditory relays), mice were anesthetized with intraperitoneal injection of xylazine (6 mg/ml, Rompun Bayer) and ketamine (80 mg/ml, Virbac) mixture diluted in physiological saline. The mouse was placed in a closed acoustic chamber and its body temperature was kept constant at 37°C during ABRs recording. For sound stimulus generation and data acquisition, we used a TDT RZ6/BioSigRZ system (Tucker-Davis Technologies). Click-based ABR signals were averaged after the presentation of a series of 512 stimulations. Thresholds were defined as the lowest stimulus for recognizable wave-I and II. The amplitude of ABR wave-I was estimated by measuring the voltage difference between the positive (P1) and negative (N1) peak of wave-I. Sound intensities of 10–90 dB SPL in 10 dB step, were tested.

Distortion product otoacoustic emissions (DPOAEs), which originate from the electromechanical activity of the outer hair cells (OHCs), were tested by using two simultaneous continuous pure tones with frequency ratio of 1.2 ( $f_1 = 12.73$  kHz and  $f_2 = 15.26$  kHz). DPOAEs were collected with the TDT RZ6/BioSigRZ system designed to measure the level of the “cubic difference tone”  $2f_1 - f_2$ .

### Acoustic Startle Reflex Measurements

Testing was conducted in four acoustic startle chambers for mice (SR-LAB, San Diego Instruments, San Diego, CA). Each chamber consisted of a nonrestrictive cylindrical enclosure attached horizontally on a mobile platform, which was in turn resting on a solid base inside a sound-attenuated isolation cubicle. A high-frequency loudspeaker mounted directly above the animal enclosure inside each cubicle produced a continuous background noise of 65 dBA and various acoustic stimuli in the form of white noise. Mechanical vibrations caused by the startle response of the mouse were converted into analog signals by a piezoelectric accelerometer attached to the platform. A total of 130 readings were taken at 0.5-ms intervals (i.e., spanning across 65 ms), starting at the onset of the startle stimulus. The average amplitude over the 65 ms was used to determine the stimulus reactivity. The sensitivity of the stabilimeter was routinely calibrated to ensure consistency between chambers and across sessions.

Acoustic startle reflex was assessed during a session lasting for ~30 min, in which the mice were presented with a series of discrete pulse-alone trials of different intensities and durations. Ten pulse intensities were used: 69, 73, 77, 81, 85, 90, 95, 100, 110, and 120 dBA lasting for either 20 or 40 ms (background noise level: 65 dBA). A session began when the animals were placed into the Plexiglas enclosure. The mice were acclimatized to the apparatus for 2 min before the first trial began. The first six trials consisted of six pulse-alone trials of 120 dBA, comprising three trials of each duration. These trials served to stabilize the animals' startle response, and were analyzed separately. Subsequently, the animals were presented with five blocks of discrete test trials. Each block consisted of 20 pulse alone trials, one for each intensity and duration. All trials were presented in a pseudorandom order with an inter-trials interval of 14 s.

## Tissue Preparation and Immunocytochemistry

Mice were deeply anesthetized with isoflurane (Vetflurane, Virbac). The ramps of the cochlear apparatus were dissected and prepared as previously described by Vincent et al. (2014). Inner ears (cochleae) were fixed by incubation in 4% paraformaldehyde in phosphate-buffered saline (PBS), pH 7.4, at 4°C overnight and washed with cold phosphate buffered saline (PBS). They were then incubated for 2 days in PBS solution containing 10% EDTA pH 7.4 at 4°C. The middle part of the organ of Corti (area encoding between 8 and 16 kHz) was then dissected and the tectorial membrane removed. The tissue was first incubated with PBS containing 30% normal horse serum and triton X100 0.5 % for 1 h at room temperature. Synaptic ribbons were labeled with anti-CtBP2 (1/200 Goat polyclonal, Santa Cruz, USA; cat # SC-5966 or 1/200 Mouse IgG1 monoclonal antibody BD Biosciences, cat # 612044). Otoferlin was labeled with a mouse monoclonal antibody (1/200 AbCam, cat # ab53233). Autophagy was detected by labeling LC3B protein with anti-Rabbit monoclonal antibody [1/200 LC3B(D11) XP, Cell Signaling Technology, cat # 3868]. BK channels were labeled with a Rabbit polyclonal antibody (1/200, Alomone, Israel, cat # APC-021). Explants of Organ of Corti were incubated overnight at 4°C with primary antibodies. The following fluorescent secondary antibodies 1/500 were then used: anti-Goat Donkey polyclonal Fluorophores 547H (Interchim, cat# FP-SB2110), anti-Mouse Donkey polyclonal Fluorophores 647H (Interchim, cat# FP-SC4110), anti-Mouse Donkey polyclonal Alexa Fluor 488 (AbCam, cat# ab150109), anti-Mouse Goat polyclonal Alexa Fluor 546 (Molecular Probes, cat# A-11003), anti-Mouse Goat polyclonal Alexa Fluor 488 (Molecular Probes, cat# A-10680), anti-Rabbit Donkey polyclonal Fluorophores 594 (Interchim, cat# FP-SD5110). Actin-F was also used to visualize hair cells (1/100, Phalloidin Fluorophore 405, Interchim, Montlucon, France; cat # FP-CA9870). For Image Acquisition, organ of Corti samples were analyzed using a confocal laser scanning microscope Leica SP8 with a 63X oil immersion objective (NA = 1.4) and white light laser (470–670 nm) (Bordeaux Imaging Center). Phalloidin was imaged by using a diode laser at 405 nm also mounted on the microscope. For complete 3D-stack reconstruction of IHCs, 25–30 images (0.3 μm thickness) were acquired as previously described (Vincent et al., 2014). Ribbon volumes were calculated using the 3D-Objects Counter Plugin of ImageJ. Image resolution was 0.038 μm/pixel. As previously described by Hickman et al. (2020) and Jeng et al. (2020), the *x,y,z* coordinates of ribbons in each *z*-stack were transformed into a coordinate system based on the modiolar-pillar polarity of the IHCs. We determined the pillar vs. modiolar distribution of the synaptic ribbons by using a *k*-means clustering method in the *z*-stack position of each ribbon, with arbitrarily choosing the number of clusters as 2 (OriginPro 9.1 software, OriginLab, Northampton, USA). From these two clusters, we determine arbitrarily the border between the modiolar and pillar side in each IHC by taking the half-distance between the two nearest ribbon of each cluster.

## High Resolution Imaging of Synaptic Ribbons With Confocal STED Microscopy

For high-resolution imaging of IHC ribbons, we used a Leica DMI6000 TCS SP8 STED microscope with 93X glycerol immersion objective (NA 1.3) (Bordeaux Imaging Center). Mouse sensory organs were fixed and incubated with primary anti CtBP2 (1/100) antibodies in conditions similar to those described above for confocal microscopy. Secondary antibodies Goat anti- IgG1 Mouse polyclonal Alexa Fluor 647 (Jackson, cat# 115-605-205) were used to label CtBP2 primary antibodies. The pulsed STED depletion laser (pulsed laser IR, Spectra Physics Mai Tai) was set at 775 nm. Stack images were acquired with the following parameters: scan rate 200 Hz, 775 nm depletion laser power between 8 and 15%, scans frames accumulated per *X–Y* section 8 times, *z*-step size 0.25 μm, number of plans between 8 and 10, pixel size 20 nm giving an *X–Y* image size of 21 × 5 μm (1,024 × 256 pixels).

## Counting Spiral Ganglion Neurons

The afferent nerve fibers of the auditory nerve were fluorescently labeled using a retrograde track tracing technique with dextran amines (Fritzsch et al., 2016). Cochleae were extracted from temporal bone of freshly euthanized mice and rapidly immersed intact into ice-cold artificial perilymph (NaCl 135; KCl 5.8; CaCl<sub>2</sub> 1.3; MgCl<sub>2</sub> 0.9; NaH<sub>2</sub>PO<sub>4</sub> 0.7; Glucose 5.6; Na pyruvate 2; HEPES 10, pH 7.4, 305 mOsm). A small crystal of tetramethyl rhodamine dextran amines 3000 (Life technologies, NY) was placed for 15–20 min at the edge of the auditory nerve coming out at the internal auditory canal of the intact cochlea and rinsed with artificial perilymph. The intracochlear sensory tissues were then fixed by gentle perfusion of a 4% PFA solution for 30 min and rinsed with PBS. They were then decalcified for 2 days in PBS solution containing 10% EDTA pH 7.4 at 4°C. The cochleae were then sliced with a razor blade along the longitudinal cochlear axes and the slices were then mounted on a glass-slide for fluorescent confocal microscopy observation. The quantification of the spiral ganglion neurons per surface area of the neural ganglion were made in the middle part of the cochlea in a region encoding 8–16 kHz, by using the 3D object counter application of ImageJ software.

## Ca<sup>2+</sup> Currents and Whole-Cell Membrane Capacitance Measurement in IHCs

Measurements of resting membrane capacitance of IHCs were performed at P30 and P365 mice in the 20–40% normalized distance from the apex, an area coding for frequencies ranging from 8 to 16 kHz, by using an EPC10 amplifier controlled by Patchmaster pulse software (HEKA Elektronik, Germany), as previously described in detail (Vincent et al., 2014, 2015). The organ of Corti was incubated in an extracellular perilymph-like solution containing NaCl 135; KCl 5.8; CaCl<sub>2</sub> 5; MgCl<sub>2</sub> 0.9; NaH<sub>2</sub>PO<sub>4</sub> 0.7; Glucose 5.6; Na pyruvate 2; HEPES 10, pH 7.4, 305 mOsm. This extracellular solution was complemented with 0.25 μM of apamin (Latoxan; cat # L8407) and 1 μM of XE-991 (Tocris Bioscience; cat # 2000) to block SK channels and KCNQ4 channels, respectively. The external Ca<sup>2+</sup> concentration was

increased from 1.3 to 5 mM to enhance the amplitude of  $\text{Ca}^{2+}$  currents to levels nearby body temperature. All experiments were performed at room temperature (22–24°C).

Patch pipettes were pulled with a micropipette Puller P-97 Flaming/Brown (Sutter Instrument, Novato, CA, USA) and fire-polished with a Micro forge MF-830 (Narishige, Japan) to obtain a resistance range from 3 to 5 M $\Omega$ . Patch pipettes were filled with a cesium-based intracellular solution containing (in mM): CsCl 145; MgCl<sub>2</sub> 1; HEPES 5; EGTA 1; TEA 20; ATP 2, GTP 0.3, pH 7.2, 300 mOsm. Measurements of the resting membrane capacitance (cell size) of IHCs were obtained in whole-cell voltage-clamp configuration at –70 mV and after 2 min equilibrium of the internal patch-pipette recording solution with the IHC cytosol.

## BK Currents

Whole-cell recordings of BK currents were recorded in P30 and P365 IHCs from *ex-vivo* whole-mount preparation (Skinner et al., 2003) as described above for  $\text{Ca}^{2+}$  currents. Recording pipettes were filled with a KCl-based intracellular solution containing in mM: 158 KCl, 2 MgCl<sub>2</sub>, 1.1 EGTA, 5 HEPES, and 3.05 KOH, pH 7.20.

## Intracellular $\text{Ca}^{2+}$ Imaging

Fluorescent  $\text{Ca}^{2+}$  signals were measured with a C2 confocal system and NIS-element imaging software (Nikon) coupled to the FN1 upright microscope as previously described (Vincent et al., 2014, 2017). For  $\text{Ca}^{2+}$  imaging in IHCs, in which membrane capacitance and  $\text{Ca}^{2+}$  currents were simultaneously recorded, patch pipettes were filled with the same cesium-base solution described above supplemented with 50  $\mu\text{M}$  of the red fluorescent indicator Rhod2 (R14220, Invitrogen™, Thermofisher Scientific). The  $\text{Ca}^{2+}$  dye was excited with a 543 nm Helium Neon Laser system (Melles Griot 05-LGR-193-381) coupled to a Nikon C2-confocal FN1- upright microscope and emission fluorescence at 552–617 nm was recorded at 18 images/s (resolution 0.4  $\mu\text{m}/\text{pixel}$ ). Using the Nikon imaging system NIS-Elements, IHC active zones were first individually identified by their fluorescent transient responses, following a 100 ms stimulation (from –80 to –10 mV) and then the focal plane (with pinhole 1.1  $\mu\text{m}$ ) was adjusted in the z dimension to give the brightest value for each active zone. Then, after a 1 min rest, each active zone was stimulated by a train of five consecutive 100 ms stimulation, each separated by 250 ms. Fluorescence emission in each active zone was subsequently measured with ImageJ software by drawing a region of interest

of 1  $\mu\text{m}^2$  at the synaptic zone (**Figure 8A**). Emission fluorescent signals were analyzed and normalized by the ratio  $\Delta F/F_0$  ratio, where  $F_0$  was the fluorescence level before stimulation.

## Statistical Analysis

Results were analyzed with OriginPro 9.1 software (OriginLab, Northampton, USA). Data were tested for normal distribution using the Shapiro–Wilk normality test, and parametric or nonparametric tests were applied accordingly. For statistical analyses with two data sets, two-tailed unpaired *t*-tests or two-sided Mann–Whitney tests were used. For comparisons of more than two data sets, one-way ANOVA or two-way ANOVA followed by Tukey multiple comparison test were used when data was normally distributed. If a data set was not normally distributed Kruskal–Wallis tests followed by Dunn multiple comparison tests, respectively, was used. When more than two data sets were compared and significant differences were found, reported *p*-values correspond to the *post-hoc* multiple comparison test. Values of *p* < 0.05 were considered significant. Results are expressed as mean  $\pm$  SEM.

## DATA AVAILABILITY STATEMENT

The raw data supporting the conclusions of this article will be made available by the authors, without undue reservation.

## ETHICS STATEMENT

The animal study was reviewed and approved by Ethic Committee University of Bordeaux CEEA50.

## AUTHOR CONTRIBUTIONS

DD designed research and wrote the paper. SB, TP, YB, and DD performed research and analyzed the data. SP performed the Acoustic Startle Experiments. All authors contributed to the article and approved the submitted version.

## FUNDING

This work was supported by a grant from the Fondation Pour l'Audition to DD (Starting Grant FPA IDA09 2019-2024, CLINICAL TRANSLA–010703E), and from the French Society of Audioprosthesis professionals, Entendre SAS (Saint Cyr l'Ecole 78210 France). Part of the content of the manuscript has previously appeared as a preprint online at bioRxiv <https://doi.org/10.1101/2020.05.15.097550>.

## REFERENCES

- Bamji, S. X. (2005). Cadherins: actin with the cytoskeleton to form synapses. *Neuron* 47, 175–8. doi: 10.1016/j.neuron.2005.06.024
- Bartolome, M. V., del, C. E., Lopez, L. M., Carricondo, F., Poch-Broto, J., and Gil-Loyaga, P. (2002). Effects of aging on C57BL/6J mice: an electrophysiological and morphological study. *Adv. Otorhinolaryngol.* 59, 106–111. doi: 10.1159/000059247
- Becker, L., Schnee, M. E., Niwa, M., Sun, W., Maxeiner, S., Talaei, S., et al. (2018). The presynaptic ribbon maintains vesicle populations at the hair cell afferent fiber synapse. *Elife* 7:e30241. doi: 10.7554/eLife.30241
- Beurg, M., Michalski, N., Safieddine, S., Bouleau, Y., Schneggenburger, R., Chapman, E. R., et al. (2010). Control of exocytosis by synaptotagmins and otoferlin in auditory hair cells. *J. Neurosci.* 30, 13281–13290. doi: 10.1523/JNEUROSCI.2528-10.2010
- Bolz, H., Reiners, J., Wolfrum, U., and Gal, A. (2002). “The role of cadherins in  $\text{Ca}^{2+}$ -mediated cell adhesion and inherited photoreceptor degeneration,” in

- Photoreceptors and Calcium*, Vol. 514, *Advances in Experimental Medicine and Biology*, eds. W. Baehr and K. Palczewski (Boston, MA: Springer), 399–410.
- Brandt, A., Striessnig, J., and Moser, T. (2003). CaV1.3 channels are essential for development and presynaptic activity of cochlear inner hair cells. *J. Neurosci.* 23, 10832–10840. doi: 10.1523/JNEUROSCI.23-34-10832.2003
- Campbell, L. W., Hao, S. Y., Thibault, O., Blalock, E. M., and Landfield, P. W. (1996). Aging changes in voltage-gated calcium currents in hippocampal CA1 neurons. *J. Neurosci.* 16, 6286–6295. doi: 10.1523/JNEUROSCI.16-19-06286.1996
- Defourny, J., Aghaie, A., Perfettini, I., Avan, P., Delmaghani, S., and Petit, C. (2019). Pejvakin-mediated pexophagy protects auditory hair cells against noise-induced damage. *Proc. Natl. Acad. Sci. U. S. A.* 116, 8010–8017. doi: 10.1073/pnas.1821844116
- Del Nido, P. J., Glynn, P., Buenaventura, P., Salama, G., and Koretsky, A. P. (1998). Fluorescence measurement of calcium transients in perfused rabbit heart using rhod 2. *Am. J. Physiol.* 274, H728–H741. doi: 10.1152/ajpheart.1998.274.2.H728
- Delmaghani, S., Defourny, J., Aghaie, A., Beurg, M., Dulon, D., Thelen, N., et al. (2015). Hypervulnerability to sound exposure through impaired adaptive proliferation of peroxisomes. *Cell* 163, 894–906. doi: 10.1016/j.cell.2015.10.023
- Fernandez, K. A., Jeffers, P. W., Lall, K., Liberman, M. C., and Kujawa, S. G. (2015). Aging after noise exposure: acceleration of cochlear synaptopathy in “recovered” ears. *J. Neurosci.* 35, 7509–7520. doi: 10.1523/JNEUROSCI.5138-14.2015
- Fingar, D. C., Salama, S., Tsou, C., Harlow, E., and Blenis, J. (2002). Mammalian cell size is controlled by mTOR and its downstream targets S6K1 and 4EBP1/eIF4E. *Genes Dev.* 16, 1472–1487. doi: 10.1101/gad.995802
- Frank, T., Khimich, D., Neef, A., and Moser, T. (2009). Mechanisms contributing to synaptic Ca<sup>2+</sup> signals and their heterogeneity in hair cells. *Proc. Natl. Acad. Sci. U. S. A.* 106, 4483–4488. doi: 10.1073/pnas.0813213106
- Fritzsch, B., Duncan, J. S., Kersigo, J., Gray, B., and Elliott, K. L. (2016). Neuroanatomical tracing techniques in the ear: history, state of the art, and future developments. *Methods Mol. Biol.* 1427, 243–262. doi: 10.1007/978-1-4939-3615-1\_14
- Fu, X., Sun, X., Zhang, L., Jin, Y., Chai, R., Yang, L., et al. (2018). Tuberosclerosis complex-mediated mTORC1 overactivation promotes age-related hearing loss. *J. Clin. Invest.* 128, 4938–4955. doi: 10.1172/JCI98058
- Fumarola, C., La Monica, S., Alfieri, R. R., Borra, E., and Guidotti, G. G. (2005). Cell size reduction induced by inhibition of the mTOR/S6K-signaling pathway protects Jurkat cells from apoptosis. *Cell Death Differ.* 12, 1344–1357. doi: 10.1038/sj.cdd.4401660
- Grant, L., and Fuchs, P. (2008). Calcium- and calmodulin-dependent inactivation of calcium channels in inner hair cells of the rat cochlea. *J. Neurophysiol.* 99, 2183–2193. doi: 10.1152/jn.01174.2007
- Graydon, C. W., Cho, S., Li, G. L., Kachar, B., and von Gersdorff, H. (2011). Sharp Ca<sup>2+</sup>(+) nanodomains beneath the ribbon promote highly synchronous multivesicular release at hair cell synapses. *J. Neurosci.* 31, 16637–16650. doi: 10.1523/JNEUROSCI.1866-11.2011
- Hafidi, A., Beurg, M., and Dulon, D. (2005). Localization and developmental expression of BK channels in mammalian cochlear hair cells. *Neuroscience* 130, 475–484. doi: 10.1016/j.neuroscience.2004.09.038
- Hasson, T., Heintzelman, M. B., Santos-Sacchi, J., Corey, D. P., and Mooseker, M. S. (1995). Expression in cochlea and retina of myosin VIIa, the gene product defective in Usher syndrome type 1B. *Proc. Natl. Acad. Sci. U. S. A.* 92, 9815–9819. doi: 10.1073/pnas.92.21.9815
- Henry, K. R. (2002). Sex- and age-related elevation of cochlear nerve envelope response (CNER) and auditory brainstem response (ABR) thresholds in C57BL/6 mice. *Hear. Res.* 170, 107–115. doi: 10.1016/S0378-5955(02)00391-X
- Hequembourg, S., and Liberman, M. C. (2001). Spiral ligament pathology: a major aspect of age-related cochlear degeneration in C57BL/6 mice. *J. Assoc. Res. Otolaryngol.* 2, 118–129. doi: 10.1007/s101620010075
- Hermann, A., Sitdikova, G. F., and Weiger, T. M. (2015). Oxidative stress and maxi calcium-activated potassium (BK) channels. *Biomolecules* 5, 1870–1911. doi: 10.3390/biom5031870
- Hickman, T. T., Hashimoto, K., Liberman, L. D., and Liberman, M. C. (2020). Synaptic migration and reorganization after noise exposure suggests regeneration in a mature mammalian cochlea. *Sci. Rep.* 10:19945. doi: 10.1038/s41598-020-76553-w
- Hu, N., Rutherford, M. A., and Green, S. H. (2020). Protection of cochlear synapses from noise-induced excitotoxic trauma by blockade of Ca<sup>2+</sup>-permeable AMPA receptors. *Proc. Natl. Acad. Sci. U. S. A.* 117, 3828–3838. doi: 10.1073/pnas.1914247117
- Ison, J. R., and Allen, P. D. (2003). Low-frequency tone pips elicit exaggerated startle reflexes in C57BL/6J mice with hearing loss. *J. Assoc. Res. Otolaryngol.* 4, 495–504. doi: 10.1007/s10162-002-3046-2
- Ison, J. R., Allen, P. D., and O'Neill, W. E. (2007). Age-related hearing loss in C57BL/6J mice has both frequency-specific and non-frequency-specific components that produce a hyperacusis-like exaggeration of the acoustic startle reflex. *J. Assoc. Res. Otolaryngol.* 8, 539–550. doi: 10.1007/s10162-007-0098-3
- Jean, P., Lopez de la Morena, D., Michanski, S., Jaime Tobon, L. M., Chakrabarti, R., Picher, M. M., et al. (2018). The synaptic ribbon is critical for sound encoding at high rates and with temporal precision. *Elife* 7:e29275. doi: 10.7554/eLife.29275
- Jeng, J. Y., Carlton, A. J., Johnson, S. L., Brown, S. D. M., Holley, M. C., Bowl, M. R., et al. (2021). Biophysical and morphological changes in inner hair cells and their efferent innervation in the ageing mouse cochlea. *J. Physiol.* 599, 269–287. doi: 10.1113/JP280256
- Jeng, J. Y., Ceriani, F., Olt, J., Brown, S. D. M., Holley, M. C., Bowl, M. R., et al. (2020). Pathophysiological changes in inner hair cell ribbon synapses in the ageing mammalian cochlea. *J. Physiol.* 598, 4339–4355. doi: 10.1113/JP280018
- Jiang, X. W., Li, X. R., and Zhang, Y. P. (2015). Changes of ribbon synapses number of cochlear hair cells in C57BL/6J mice with age(Delta). *Int. J. Clin. Exp. Med.* 8, 19058–19064.
- Jing, Z., Rutherford, M. A., Takago, H., Frank, T., Fejtova, A., Khimich, D., et al. (2013). Disruption of the presynaptic cytomatrix protein bassoon degrades ribbon anchorage, multiquantal release, and sound encoding at the hair cell afferent synapse. *J. Neurosci.* 33, 4456–4467. doi: 10.1523/JNEUROSCI.3491-12.2013
- Johnson, K. R., Erway, L. C., Cook, S. A., Willott, J. F., and Zheng, Q. Y. (1997). A major gene affecting age-related hearing loss in C57BL/6J mice. *Hear. Res.* 114, 83–92. doi: 10.1016/S0378-5955(97)00155-X
- Johnson, S. L., Marcotti, W., and Kros, C. J. (2005). Increase in efficiency and reduction in Ca<sup>2+</sup> dependence of exocytosis during development of mouse inner hair cells. *J. Physiol.* 563(Pt 1), 177–191. doi: 10.1113/jphysiol.2004.074740
- Kazmierczak, P., Sakaguchi, H., Tokita, J., Wilson-Kubalek, E. M., Milligan, R. A., Muller, U., et al. (2007). Cadherin 23 and protocadherin 15 interact to form tip-link filaments in sensory hair cells. *Nature* 449, 87–91. doi: 10.1038/nature06091
- Knipper, M., Van Dijk, P., Nunes, I., Rüttiger, L., and Zimmermann, U. (2013). Advances in the neurobiology of hearing disorders: recent developments regarding the basis of tinnitus and hyperacusis. *Prog. Neurobiol.* 111, 17–33. doi: 10.1016/j.pneurobio.2013.08.002
- Kros, C. J., Ruppersberg, J. P., and Rusch, A. (1998). Expression of a potassium current in inner hair cells during development of hearing in mice. *Nature* 394, 281–284. doi: 10.1038/28401
- Kujawa, S. G., and Liberman, M. C. (2015). Synaptopathy in the noise-exposed and aging cochlea: primary neural degeneration in acquired sensorineural hearing loss. *Hear. Res.* 330(Pt B), 191–199. doi: 10.1016/j.heares.2015.02.009
- Kujawa, S. G., and Liberman, M. C. (2019). Translating animal models to human therapeutics in noise-induced and age-related hearing loss. *Hear. Res.* 377, 44–52. doi: 10.1016/j.heares.2019.03.003
- Kurt, S., Sausbier, M., Rüttiger, L., Brandt, N., Moeller, C. K., Kindler, J., et al. (2012). Critical role for cochlear hair cell BK channels for coding the temporal structure and dynamic range of auditory information for central auditory processing. *FASEB J.* 26, 3834–3843. doi: 10.1096/fj.11-200535
- Lagziel, A., Ahmed, Z. M., Schultz, J. M., Morell, R. J., Belyantseva, I. A., and Friedman, T. B. (2005). Spatiotemporal pattern and isoforms of cadherin 23 in wild type and waltzer mice during inner ear hair cell development. *Dev. Biol.* 280, 295–306. doi: 10.1016/j.ydbio.2005.01.015

- Lang, I., Jung, M., Niemeyer, B. A., Ruth, P., and Engel, J. (2019). Expression of the LRRC52 gamma subunit (gamma2) may provide Ca(2+)-independent activation of BK currents in mouse inner hair cells. *FASEB J.* 33, 11721–11734. doi: 10.1096/fj.201900701RR
- Lieberman, L. D., Wang, H., and Liberman, M. C. (2011). Opposing gradients of ribbon size and AMPA receptor expression underlie sensitivity differences among cochlear-nerve/hair-cell synapses. *J. Neurosci.* 31, 801–808. doi: 10.1523/JNEUROSCI.3389-10.2011
- Lieberman, M. C. (1982). Single-neuron labeling in the cat auditory nerve. *Science* 216, 1239–1241. doi: 10.1126/science.7079757
- Lieberman, M. C., and Kujawa, S. G. (2017). Cochlear synaptopathy in acquired sensorineural hearing loss: manifestations and mechanisms. *Hear. Res.* 349, 138–147. doi: 10.1016/j.heares.2017.01.003
- Lingle, C. J., Martinez-Espinosa, P. L., Yang-Hood, A., Boero, L. E., Payne, S., Persic, D., et al. (2019). LRRC52 regulates BK channel function and localization in mouse cochlear inner hair cells. *Proc. Natl. Acad. Sci. U. S. A.* 116, 18397–18403. doi: 10.1073/pnas.1907065116
- Magupalli, V. G., Schwarz, K., Alpadi, K., Natarajan, S., Seigel, G. M., and Schmitz, F. (2008). Multiple RIBEYE-RIBEYE interactions create a dynamic scaffold for the formation of synaptic ribbons. *J. Neurosci.* 28, 7954–7967. doi: 10.1523/JNEUROSCI.1964-08.2008
- Matsubara, A., Laake, J. H., Davanger, S., Usami, S., and Ottersen, O. P. (1996). Organization of AMPA receptor subunits at a glutamate synapse: a quantitative immunogold analysis of hair cell synapses in the rat organ of Corti. *J. Neurosci.* 16, 4457–4467. doi: 10.1523/JNEUROSCI.16-14-04457.1996
- Meyer, A. C., Frank, T., Khimich, D., Hoch, G., Riedel, D., Chapochnikov, N. M., et al. (2009). Tuning of synapse number, structure and function in the cochlea. *Nat. Neurosci.* 12, 444–453. doi: 10.1038/nn.2293
- Michalski, N., Goutman, J. D., Auclair, S. M., Boutet de Monvel, J., Tertrais, M., Emptoz, A., et al. (2017). Otoferlin acts as a Ca(2+) sensor for vesicle fusion and vesicle pool replenishment at auditory hair cell ribbon synapses. *Elife* 6:e31013. doi: 10.7554/eLife.31013.024
- Michel, V., Goodyear, R. J., Weil, D., Marcotti, W., Perfettini, I., Wolftrum, U., et al. (2005). Cadherin 23 is a component of the transient lateral links in the developing hair bundles of cochlear sensory cells. *Dev. Biol.* 280, 281–294. doi: 10.1016/j.ydbio.2005.01.014
- Neef, J., Urban, N. T., Ohn, T. L., Frank, T., Jean, P., Hell, S. W., et al. (2018). Quantitative optical nanophysiology of Ca(2+) signaling at inner hair cell active zones. *Nat. Commun.* 9:290. doi: 10.1038/s41467-017-02612-y
- Noben-Trauth, K., Zheng, Q. Y., and Johnson, K. R. (2003). Association of cadherin 23 with polygenic inheritance and genetic modification of sensorineural hearing loss. *Nat. Genet.* 35, 21–23. doi: 10.1038/ng1226
- Oliver, D., Taberner, A. M., Thurm, H., Sausbier, M., Arntz, C., Ruth, P., et al. (2006). The role of BKCa channels in electrical signal encoding in the mammalian auditory periphery. *J. Neurosci.* 26, 6181–6189. doi: 10.1523/JNEUROSCI.1047-06.2006
- Ouagazzal, A. M., Reiss, D., and Romand, R. (2006). Effects of age-related hearing loss on startle reflex and prepulse inhibition in mice on pure and mixed C57BL and 129 genetic background. *Behav. Brain Res.* 172, 307–315. doi: 10.1016/j.bbr.2006.05.018
- Ozce, O. D., and Moser, T. (2021). A sensory cell diversifies its output by varying Ca(2+) influx-release coupling among active zones. *EMBO J.* 40:e106010. doi: 10.15252/embj.2020106010
- Pujol, R., and Puel, J. L. (1999). Excitotoxicity, synaptic repair, and functional recovery in the mammalian cochlea: a review of recent findings. *Ann. N. Y. Acad. Sci.* 884, 249–254. doi: 10.1111/j.1749-6632.1999.tb08646.x
- Pyott, S. J., Glowatzki, E., Trimmer, J. S., and Aldrich, R. W. (2004). Extrasynaptic localization of inactivating calcium-activated potassium channels in mouse inner hair cells. *J. Neurosci.* 24, 9469–9474. doi: 10.1523/JNEUROSCI.3162-04.2004
- Rousset, F., Nacher-Soler, G., Coelho, M., Ilmjarv, S., Kojke, V. B. C., Marteyn, A., et al. (2020). Redox activation of excitatory pathways in auditory neurons as mechanism of age-related hearing loss. *Redox Biol.* 30:101434. doi: 10.1016/j.redox.2020.101434
- Roux, I., Safieddine, S., Nouvian, R., Grati, M., Simmler, M. C., Bahloul, A., et al. (2006). Otoferlin, defective in a human deafness form, is essential for exocytosis at the auditory ribbon synapse. *Cell* 127, 277–289. doi: 10.1016/j.cell.2006.08.040
- Sahoo, N., Hoshi, T., and Heinemann, S. H. (2014). Oxidative modulation of voltage-gated potassium channels. *Antioxid. Redox Signal.* 21, 933–952. doi: 10.1089/ars.2013.5614
- Sheets, L., He, X. J., Olt, J., Schreck, M., Petralia, R. S., Wang, Y. X., et al. (2017). Enlargement of ribbons in zebrafish hair cells increases calcium currents but disrupts afferent spontaneous activity and timing of stimulus onset. *J. Neurosci.* 37, 6299–6313. doi: 10.1523/JNEUROSCI.2878-16.2017
- Siemens, J., Lillo, C., Dumont, R. A., Reynolds, A., Williams, D. S., Gillespie, P. G., et al. (2004). Cadherin 23 is a component of the tip link in hair-cell stereocilia. *Nature* 428, 950–955. doi: 10.1038/nature02483
- Skinner, L. J., Enee, V., Beurg, M., Jung, H. H., Ryan, A. F., Hafidi, A., et al. (2003). Contribution of BK Ca2+-activated K+ channels to auditory neurotransmission in the Guinea pig cochlea. *J. Neurophysiol.* 90, 320–332. doi: 10.1152/jn.01155.2002
- Sollner, C., Rauch, G. J., Siemens, J., Geisler, R., Schuster, S. C., Muller, U., et al. (2004). Mutations in cadherin 23 affect tip links in zebrafish sensory hair cells. *Nature* 428, 955–959. doi: 10.1038/nature02484
- Spassova, M. A., Soboloff, J., He, L. P., Hewavitharana, T., Xu, W., Venkatchalam, K., et al. (2004). Calcium entry mediated by SOCs and TRP channels: variations and enigma. *Biochim. Biophys. Acta* 1742, 9–20. doi: 10.1016/j.bbamcr.2004.09.001
- Spongr, V. P., Flood, D. G., Frisina, R. D., and Salvi, R. J. (1997). Quantitative measures of hair cell loss in CBA and C57BL/6 mice throughout their life spans. *J. Acoust. Soc. Am.* 101, 3546–3553. doi: 10.1121/1.1418315
- Stamatakis, S., Francis, H. W., Lehar, M., May, B. J., and Ryugo, D. K. (2006). Synaptic alterations at inner hair cells precede spiral ganglion cell loss in aging C57BL/6J mice. *Hear. Res.* 221, 104–118. doi: 10.1016/j.heares.2006.07.014
- Taberner, A. M., and Liberman, M. C. (2005). Response properties of single auditory nerve fibers in the mouse. *J. Neurophysiol.* 93, 557–569. doi: 10.1152/jn.00574.2004
- Thibault, O., and Landfield, P. W. (1996). Increase in single L-type calcium channels in hippocampal neurons during aging. *Science* 272, 1017–1020. doi: 10.1126/science.272.5264.1017
- Vincent, P. F., Bouleau, Y., Charpentier, G., Emptoz, A., Safieddine, S., Petit, C., et al. (2017). Different CaV1.3 channel isoforms control distinct components of the synaptic vesicle cycle in auditory inner hair cells. *J. Neurosci.* 37, 2960–2975. doi: 10.1523/JNEUROSCI.2374-16.2017
- Vincent, P. F., Bouleau, Y., Petit, C., and Dulon, D. (2015). A synaptic F-actin network controls otoferlin-dependent exocytosis in auditory inner hair cells. *Elife* 4:10988. doi: 10.7554/eLife.10988.008
- Vincent, P. F., Bouleau, Y., Safieddine, S., Petit, C., and Dulon, D. (2014). Exocytotic machineries of vestibular type I and cochlear ribbon synapses display similar intrinsic otoferlin-dependent Ca2+ sensitivity but a different coupling to Ca2+ channels. *J. Neurosci.* 34, 10853–10869. doi: 10.1523/JNEUROSCI.0947-14.2014
- Walton, J. P., Frisina, R. D., and Meierhans, L. R. (1995). Sensorineural hearing loss alters recovery from short-term adaptation in the C57BL/6 mouse. *Hear. Res.* 88, 19–26. doi: 10.1016/0378-5955(95)00093-J
- Wan, G., and Corfas, G. (2015). No longer falling on deaf ears: mechanisms of degeneration and regeneration of cochlear ribbon synapses. *Hear. Res.* 329, 1–10. doi: 10.1016/j.heares.2015.04.008
- Wang, Y., Tao, J., Wang, M., Yang, L., Ning, F., Xin, H., et al. (2019). Mechanism of regulation of big-conductance Ca(2+)-activated K(+) channels by mTOR complex 2 in podocytes. *Front. Physiol.* 10:167. doi: 10.3389/fphys.2019.00167
- Willott, J. F. (1996). Anatomic and physiologic aging: a behavioral neuroscience perspective. *J. Am. Acad. Audiol.* 7, 141–151.
- Wong, H. C., Zhang, Q., Beirl, A. J., Petralia, R. S., Wang, Y. X., and Kindt, K. (2019). Synaptic mitochondria regulate hair-cell synapse size and function. *Elife* 8:e48914. doi: 10.7554/eLife.48914.sa2

- Zachary, S. P., and Fuchs, P. A. (2015). Re-emergent inhibition of cochlear inner hair cells in a mouse model of hearing loss. *J. Neurosci.* 35, 9701–9706. doi: 10.1523/JNEUROSCI.0879-15.2015
- Zheng, Q. Y., Johnson, K. R., and Erway, L. C. (1999). Assessment of hearing in 80 inbred strains of mice by ABR threshold analyses. *Hear. Res.* 130, 94–107. doi: 10.1016/S0378-5955(99)00003-9
- Zhou, X., Jen, P. H., Seburn, K. L., Frankel, W. N., and Zheng, Q. Y. (2006). Auditory brainstem responses in 10 inbred strains of mice. *Brain Res.* 1091, 16–26. doi: 10.1016/j.brainres.2006.01.107

**Conflict of Interest:** The authors declare that the research was conducted in the absence of any commercial or financial relationships that could be construed as a potential conflict of interest.

**Publisher's Note:** All claims expressed in this article are solely those of the authors and do not necessarily represent those of their affiliated organizations, or those of the publisher, the editors and the reviewers. Any product that may be evaluated in this article, or claim that may be made by its manufacturer, is not guaranteed or endorsed by the publisher.

*Copyright © 2021 Peineau, Belleudy, Pietropaolo, Bouleau and Dulon. This is an open-access article distributed under the terms of the Creative Commons Attribution License (CC BY). The use, distribution or reproduction in other forums is permitted, provided the original author(s) and the copyright owner(s) are credited and that the original publication in this journal is cited, in accordance with accepted academic practice. No use, distribution or reproduction is permitted which does not comply with these terms.*